ON PARACHUTIST DYNAMICS

Ronald L. Huston

James W. Kamman

Department of Mechanical and Industrial Engineering
University of Cincinnati
Cincinnati, Ohio 45221

Technical Report for Office of Naval Research
under Contract N00014-76C-C139

ON PARACHUTIST DYNAMICS

Ronald L. Huston

James W. Kamman

Department of Mechanical and Industrial Engineering
University of Cincinnati
Cincinnati, Ohio 45221

Technical Report for Office of Naval Research
under Contract N00014-76C-C139

80 10 9 087

(9) Final Report, 1 OCT 78 — 30 SEP 80

SECURITY CLASSIFICATION OF THIS PAGE (When Data Entered)

REPORT DOCUMENTATION PAGE	READ INSTRUCTIONS BEFORE COMPLETING FORM
1. REPORT NUMBER: UC-MIE-100180-1F - ONR	2. GOVT ACCESSION NO.: AD-A090 335
3. RECIPIENT'S CATALOG NUMBER	
4. TITLE (and Subtitle): On Parachutist Dynamics	5. TYPE OF REPORT & PERIOD COVERED: Technical 10/1/78-9/30/80
	6. PERFORMING ORG. REPORT NUMBER
7. AUTHOR(s): Ronald L. Huston, James W. Kamman	8. CONTRACT OR GRANT NUMBER(s): N00014-76C-0139
9. PERFORMING ORGANIZATION NAME AND ADDRESS: University of Cincinnati, Cincinnati, Ohio 45221	10. PROGRAM ELEMENT, PROJECT, TASK AREA & WORK UNIT NUMBERS: 122303
11. CONTROLLING OFFICE NAME AND ADDRESS: CNR Resident Research Representative, Ohio State University, 1314 Kenner Rd., Columbus, Ohio 43212	12. REPORT DATE: 10/1/80 (11 OCT 80); 13. NUMBER OF PAGES: 59
14. MONITORING AGENCY NAME & ADDRESS (if different from Controlling Office): Office of Naval Research, Structural Mechanics Code 474, Department of the Navy, Arlington, VA 22217	15. SECURITY CLASS. (of this report); 15a. DECLASSIFICATION/DOWNGRADING SCHEDULE

16. DISTRIBUTION STATEMENT (of this Report)

Distribution of this report is unlimited.

17. DISTRIBUTION STATEMENT (of the abstract entered in Block 20, if different from Report)

18. SUPPLEMENTARY NOTES

19. KEY WORDS (Continue on reverse side if necessary and identify by block number)

Parachutist Dynamics, Biodynamic Modelling, Computer Simulation, Aircraft Occupant Safety, Restraining Devices, Ejection Systems

20. ABSTRACT (Continue on reverse side if necessary and identify by block number)

The dynamics of a parachutist is discussed. Results of a computer simulation and a parameter study are presented. A variety of initial parachutist configurations prior to "opening shock" are considered and the relative effects upon the parachutist's dynamics - particularly, the head/neck system dynamics - are studied. Optimal initial (pre-opening) configurations which minimize the subsequent force and moment pulses experienced by the head/neck system, are identified and discussed. Application in parachute design and in developing jumping strategies are also discussed.

DD FORM 1 JAN 73 1473 EDITION OF 1 NOV 65 IS OBSOLETE
S/N 0102-014-6601

UNCLASSIFIED
SECURITY CLASSIFICATION OF THIS PAGE (When Data Entered)

41196

A B S T R A C T

The dynamics of a parachutist is discussed. Results of a computer simulation and a parameter study are presented. A variety of initial parachutist configurations prior to "opening shock" are considered and the relative effects upon the parachutist's dynamics -- particularly, the head/neck system dynamics -- are studied. Optimal initial (pre-opening) configurations which minimize the subsequent force and moment pulses experienced by the head/neck system, are identified and discussed. Application in parachute design and in developing jumping strategies are also discussed.

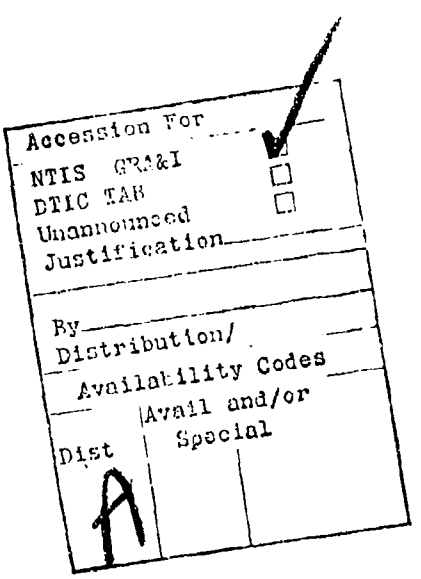

NOTATION

a_{ik} - Governing differential equation coefficients (See Equation (5).)

$\underset{\sim}{a}_j$ - Acceleration of G; in a Newtonian reference frame

A_j - Projected profile area of body B_j

B_j - A typical body of the system

C_D - Drag coefficient

$\underset{\sim}{D}_j$ - Resultant air drag force on body B_j (See Equation (1).)

f_i - Generalized force array (See Equation (5).)

$\underset{\sim}{F}_j$ - Inertia force on B_j (See Equation (3).)

G_j - Mass center of body B_j

L - Point of application of the left riser force (See Figure 1.)

m_j - Mass of B_j

$\underset{\sim}{n}_j$ - A unit vector parallel to the axis of B_j

R - Point of application of the right riser force (See Figure 2.)

V_j - Velocity of G_j relative to the air and perpendicular to the axis of body B_j (See Equation (2).)

$\underset{\sim}{V}_W$ - Ambient air velocity

X_j, Y_j, Z_j - Coordinate axes of body B_j

$\underset{\sim}{\alpha}_j$ - Angular acceleration of B_j in a Newtonian reference frame

ρ - Mass density of air

ψ_k - Generalized coordinates

$\underset{\sim}{\omega}_j$ - Angular velocity of B_j in a Newtonian reference frame

INTRODUCTION

This report presents the results of a computer-aided parameter study on parachutist dynamics. Particular attention is given to head/neck dynamics. The objective of the parameter study is to obtain optimal initial configurations, prior to opening shock, which will minimize the forces and moments experienced by the head/neck system.

During the past decade, there has been an increasing interest in parachutist dynamics during and immediately after the opening of the parachute. This interest stems from the high incidence of injuries occurring in emergency egress from high speed aircraft. Since most of the permanent disabilities are the result of injuries to the head/neck system, the major concern of researchers has been the parachutist's head/neck dynamics. These interests and concerns have stimulated the development of a number of experimental studies of parachutist response. These studies have used both volunteers and dummies in a variety of jumping configurations. A summary of some of these experiments are contained in papers by Palmer, Call, and Ewing [1,2]*. Also, studies on opening shock and parachute opening theory have been conducted by Heinrich and Saari [3]. Performance data for various types of parachute assemblies and harnesses has been tabulated by Woolman [4].

In a recent paper, Huston, Winget, and Harlow [5] suggested that it may be possible to obtain analytical simulation of parachutist dynamics

---

*Numbers in brackets refer to references at the end of the report.

by using a biodynamic computer model of the parachutist. Indeed, by using a modified version of the UCIN Crash Victim computer model [6-10], they were able to exhibit a reasonably close correspondence between analytical and experimental data. These encouraging results were a motivating factor for the parameter study summarized in this report.

The report itself is divided into three parts with the following part providing a description of the biodynamic model and the forces applied to it. This is followed by a description of the governing dynamical equations. The final part provides a summary of the results as well as conclusions regarding optimal initial configurations.

THE BIODYNAMIC PARACHUTIST MODEL

Figure 1. contains a schematic representation of the model. It consists of a system of connected rigid bodies simulating the human frame. The arms and legs are represented by frustrums of elliptical cones. The torso and neck are elliptical cylinders and the head is a spheroid. The bodies are connected by spherical joints. Nonlinear springs and dampers are used between adjacent bodies to simulate the ligaments and muscles and to limit the range of motion [7,10,11].

The model has 13 bodies and thus it has 42 degrees of freedom (3 rotational degrees of freedom for each body and a translational degree of freedom for a reference body, say B_1). This model is a modification of the model used in Reference [5]. The difference is the inclusion of a neck segment, thus improving the accuracy of the modelling.

The model allows for the arbitrary specification of external forces and moments on each of its bodies. For a parachutist, the externally-applied forces are gravity forces, the riser forces, and the wind or air drag forces. The gravity forces may be represented as vertical (downward) forces passing through the respective mass centers of the bodies. The riser forces are assumed to be applied at the shoulders at points L (left riser) and R (right riser) as shown in Figure 1. The direction of the riser forces is assumed to be opposite to the direction of the velocities of L and R relative to the air. Finally, the air drag forces are represented on each body by a single force passing through the mass center of the body and directed

opposite to the direction of the velocity of the mass center relative to the air. Specifically, if B_j is a typical body of the system as shown in Figure 2., then the air drag force $\underset{\sim}{D}_j$ on B_j is given by:

$$\underset{\sim}{D}_j = -\rho C_D A_j |\underset{\sim}{V}_j| \underset{\sim}{V}_j \qquad (1)$$

where j=1,...,13, and where ρ is the mass density of the air, C_D is the drag coefficient (dependent upon the Reynolds number), A_j is the projected profile area of B_j, and $\underset{\sim}{V}_j$ is the component of the velocity of B_j relative to the air and perpendicular to the axis of B_j. If $\underset{\sim}{V}_W$ is the ambient air velocity, $\underset{\sim}{V}_j$ is given by:

$$\underset{\sim}{V}_j = \underset{\sim}{n}_j \times [(\underset{\sim}{V}_j - \underset{\sim}{V}_W) \times \underset{\sim}{n}_j] \qquad (2)$$

where $\underset{\sim}{n}_j$ is a unit vector parallel to the axis of B_j as shown in Figure 2.

The inertia forces acting on the bodies of the model due to their motion in a Newtonian reference frame may be represented on each body B_j by a single force $\underset{\sim}{F}_j$ passing through G_j, the mass center of B_j together with a couple with torque $\underset{\sim}{T}_j$. $\underset{\sim}{F}_j$ and $\underset{\sim}{T}_j$ may be expressed as [12]:

$$\underset{\sim}{F}_j = -m_j \underset{\sim}{a}_j \qquad (3)$$

and

$$\underset{\sim}{T}_j = -\underset{\sim}{I}_j \cdot \underset{\sim}{\alpha}_j - \underset{\sim}{\omega}_j \times (\underset{\sim}{I}_j \times \underset{\sim}{\omega}_j) \qquad (4)$$

where $j=1,\ldots,13$, and where m_j is the mass of B_j, $\underline{I}_j$ is the inertia dyadic of B_j relative to G_j, $\underline{a}_j$ is the acceleration of G_j, $\underline{\omega}_j$ is the angular velocity of B_j, and $\underline{\alpha}_j$ is the angular acceleration of B_j -- all measured relative to a Newtonian reference frame.

Finally, each body B_j of the system has a coordinate axes system X_j,Y_j,Z_j $(j=1,\ldots,13)$ where X_j is forward, Y_j is to the left, and Z_j is upward. In a reference configuration of the model, as in Figure 1, the respective coordinate axes are parallel.

GOVERNING EQUATIONS

When the model is subjected to the forces outlined above, the governing dynamical equations of motion may be conveniently obtained by using Lagrange's form of d'Alembert's principle as developed by Kane et.al. [12-14]. This principle, a virtual work type principle, leads to governing equations whose coefficients are readily converted into algorithms for numerical generation on a computer. Such algorithms have been written resulting in several computer codes called UCIN[5-10,15,16]. In one of these codes, called "PARACHUTE," the governing differential equations take the form:

$$\sum_{k=1}^{42} a_{ik}\ddot{\psi}_k = f_i \qquad (i=1,\ldots,42) \qquad (5)$$

where the ψ_k (k=1,...,42) are generalized coordinates corresponding to the degrees of freedom of the system and a_{ik} and f_i are generalized inertia and force arrays. The system of Equations (5) is a coupled system of non-linear stiff ordinary differential equations. The system may be integrated numerically using a differential equation solver routine. In the current parameter study, a fourth order Runge-Kutta technique called RKGS was used to numerically integrate the equations.

RESULTS AND CONCLUSIONS

The parachutist model and its accompaning computer code described above were used in making a parameter study of a parachutist in a variety of initial configurations, prior to opening shock, for a typical low-speed jump, without ambient wind. The riser force data for the study were obtained from experimental data from volunteer jumps at the Naval Air Recovery Facility at El Centro, CA. The physical data for the parachutist model were also obtained experimentally. In the current study, it approximated that of a 75th percentile man.

The study was conducted for 3 inclinations of the spine or torso relative to the vertical and for three initial head and neck inclinations providing a total of 9 different jumping configurations. Specifically, the torso was inclined to the vertical at 22.5°, 45°, and 67.5°. The initial angle between the head and the neck and between the neck and the upper torso were equal to each other; they have the values -15°, 0°, and 15°. The initial configurations of the arms and legs were "spread-eagle" and were the same for all computer runs.

The X, Y, and Z components of the riser forces relative to a Newtonian reference frame varied only slightly with the initial configuration. Typical values are shown graphically in Figures 3., 4., and 5. Using such riser forces together with the physical parameters and the initial conditions, the coefficients of the governing differential equations were computed and the equations were numerically integrated. The results of this integration were time histories of the generalized coordinates and

their derivatives. These, in turn, were used to determine the head and neck motion and the internal restraining forces and moments on the head/neck system. Figures 6. to 17. show the resulting head rotation relative to the neck and the neck rotation relative to the upper torso for the various combinations of the initial head, neck, and torso inclination angles. The "alpha" rotation corresponds to "roll" about the X-axis and the "beta" rotation corresponds to "pitch" about the Y-axis. Figures 18. to 29. show the components and magnitude of the resultant restoring force between the head and neck for the various initial head, neck, and torso inclination angles. Figures 30. to 38. show the X and Y components and magnitude of the restraining moment between the head and neck for the various initial configurations. (The Z components of the moments were negligible.) Finally, Figures 39., 40., and 41. show the Y component of the angular acceleration of the head relative to the upper torso for each run.

A careful examination of these figures shows that there is very little difference between the results for the different initial head and neck inclination angles. However, there is a difference in the results for different initial torso inclination angles. Interestingly, it is seen in Figures 21., 25., and 29. that the smallest peak restoring force magnitude occurs with a 45° torso inclination angle. This is also the case for the magnitude of the restoring moment as seen in Figures 32., 35., and 38. Moreover, the peaks occur at approximately 40 and 80 milliseconds, which corresponds to peak values of the riser force components as seen in Figures 3., 4., and 5.

The fact that the initial torso inclination has a greater effect upon the head/neck dynamics than the head and neck inclination may not be surprising when one considers the relative magnitudes of the masses and inertias of the torso bodies and the head and neck. This may be discouraging for a parachutist, since control of the initial relative head and neck inclination is probably easier than control of the initial torso inclination. However, for designers of automatic parachute-opening devices for high-speed egress, these results may be encouraging, since torso inclination is likely to vary at a more uniform rate than the head and neck inclination.

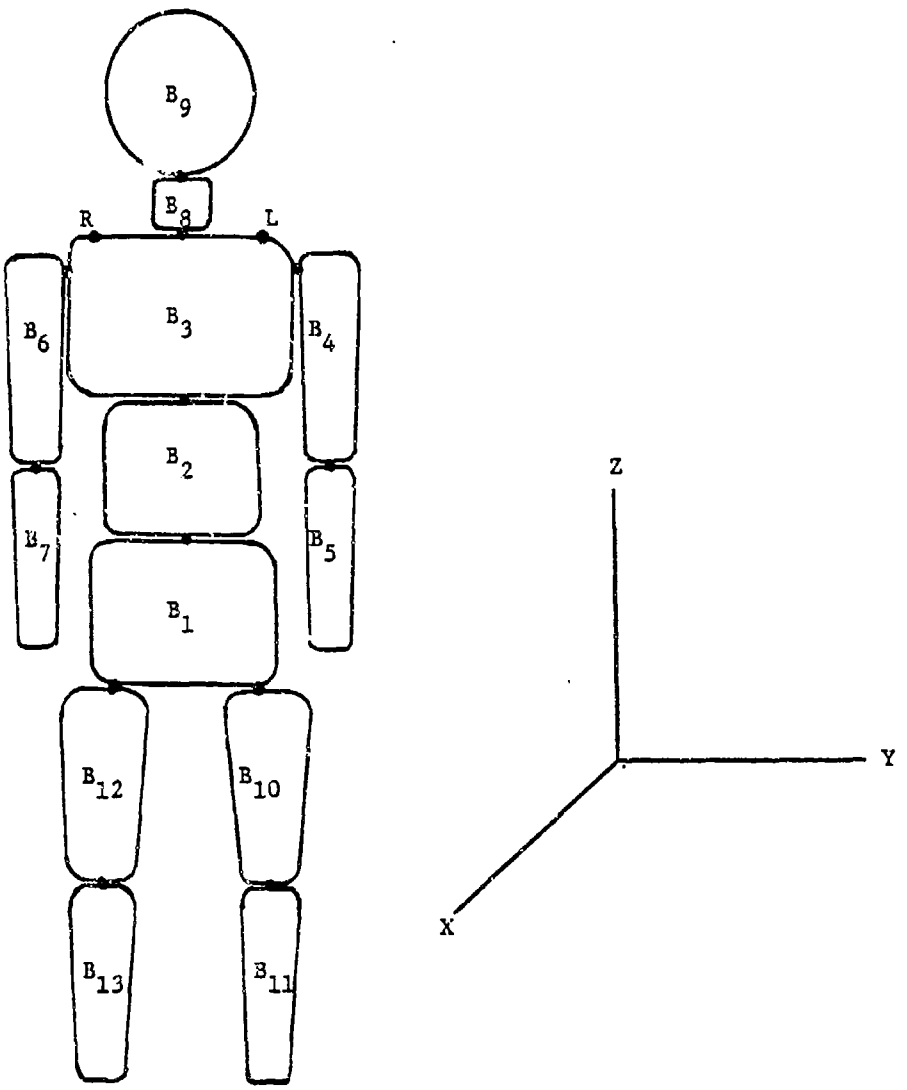

Figure 1. Biodynamic Model of a Parachutist

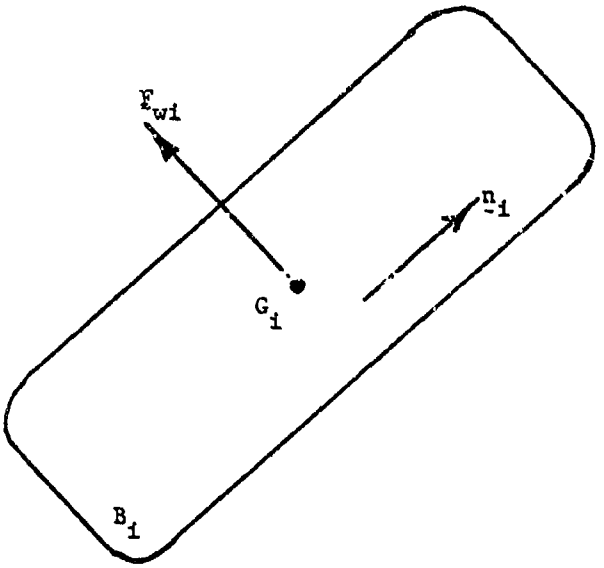

Figure 2. Air Drag Force on a Typical Body

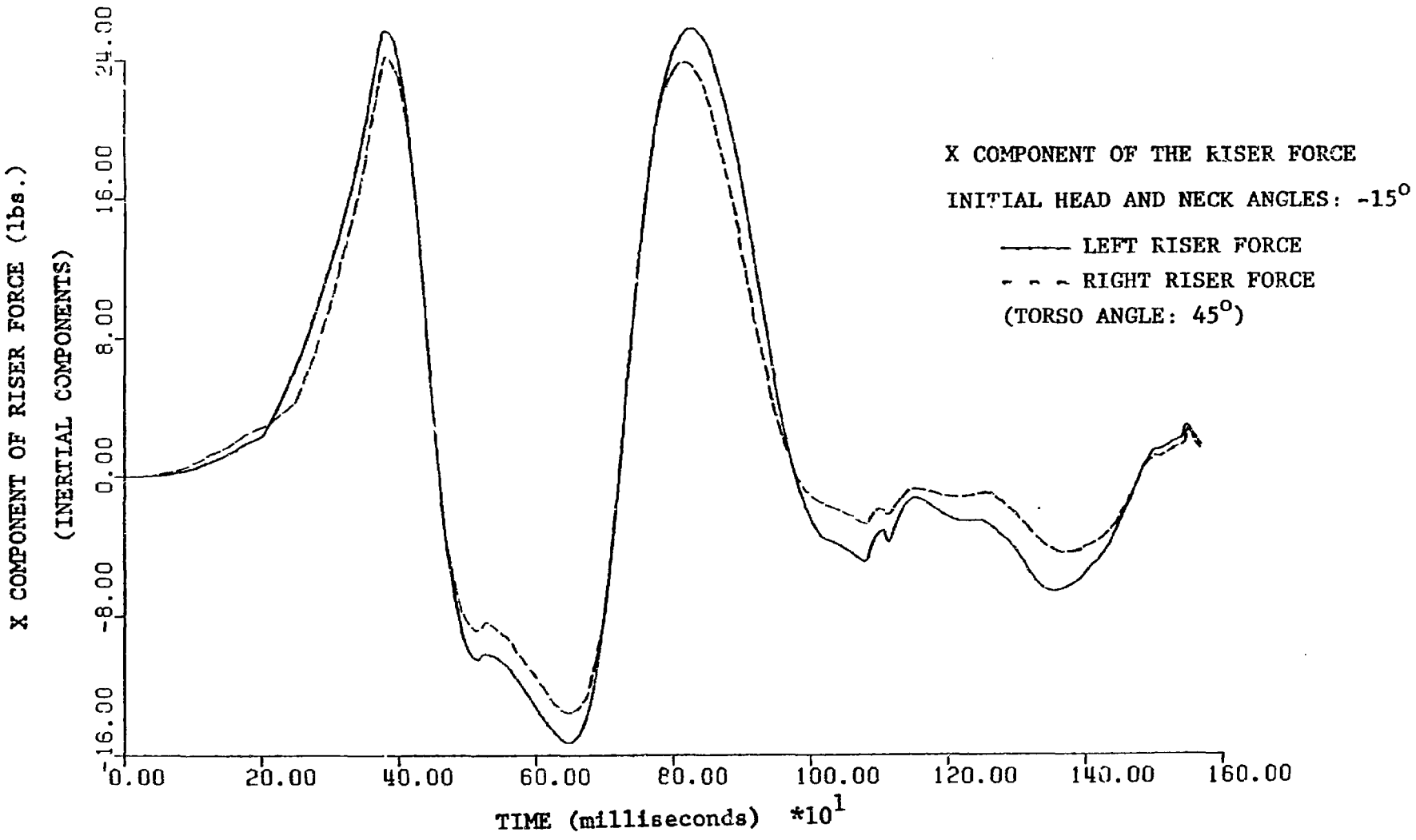

Figure 3. X Component of the Riser Force

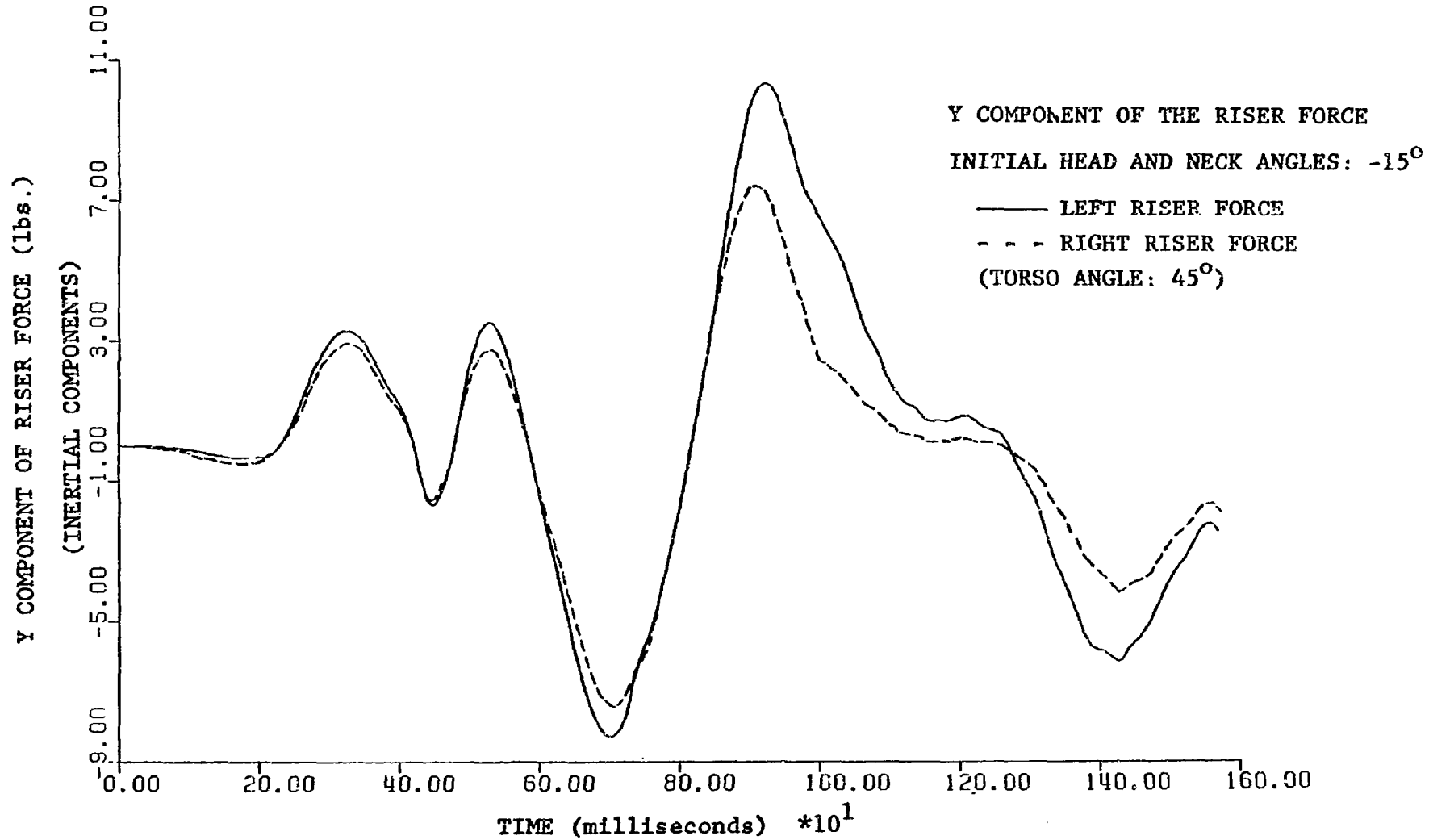

Figure 4. Y Component of the Riser Force

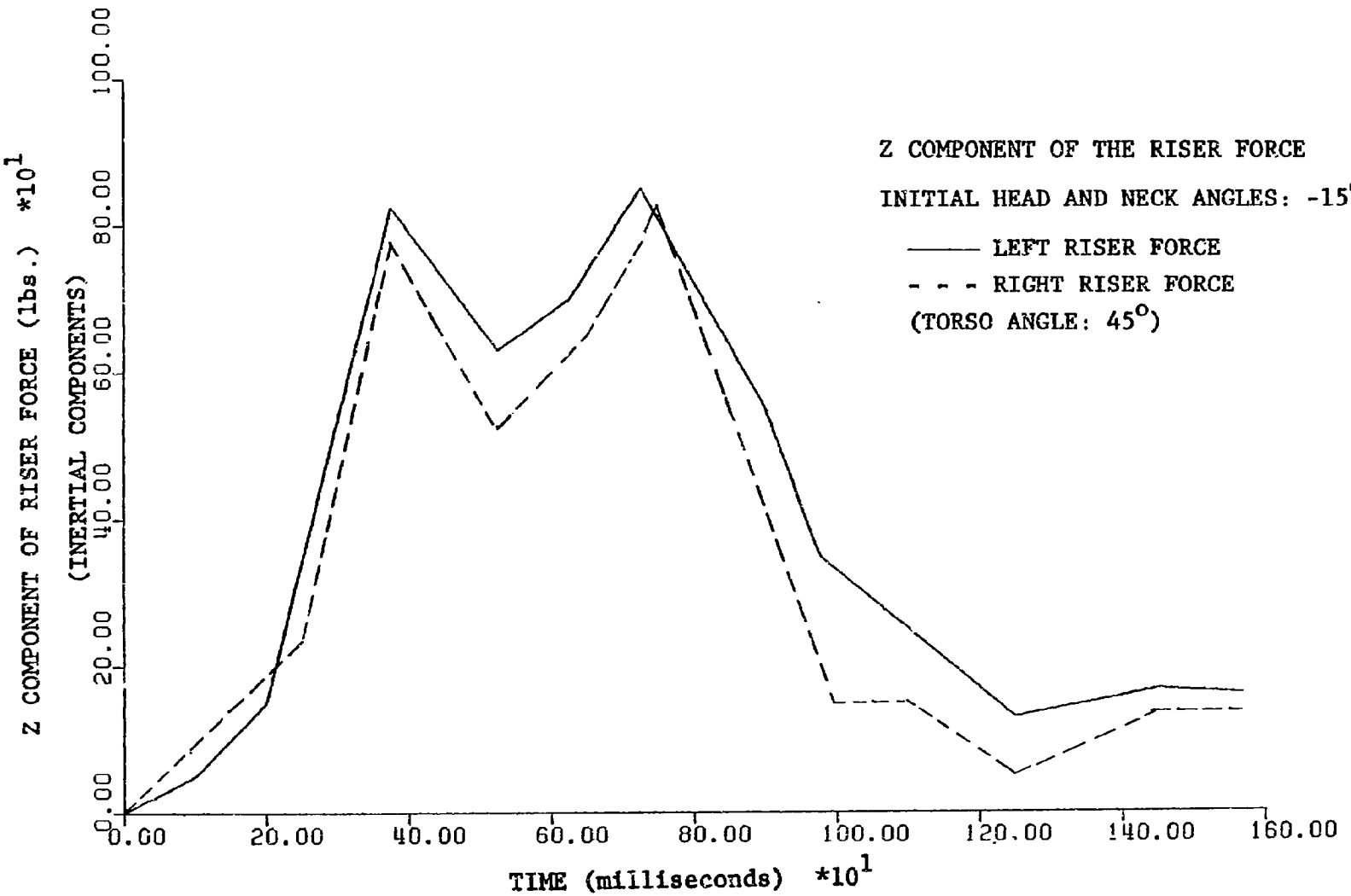

Figure 5. Z Component of the Riser Force

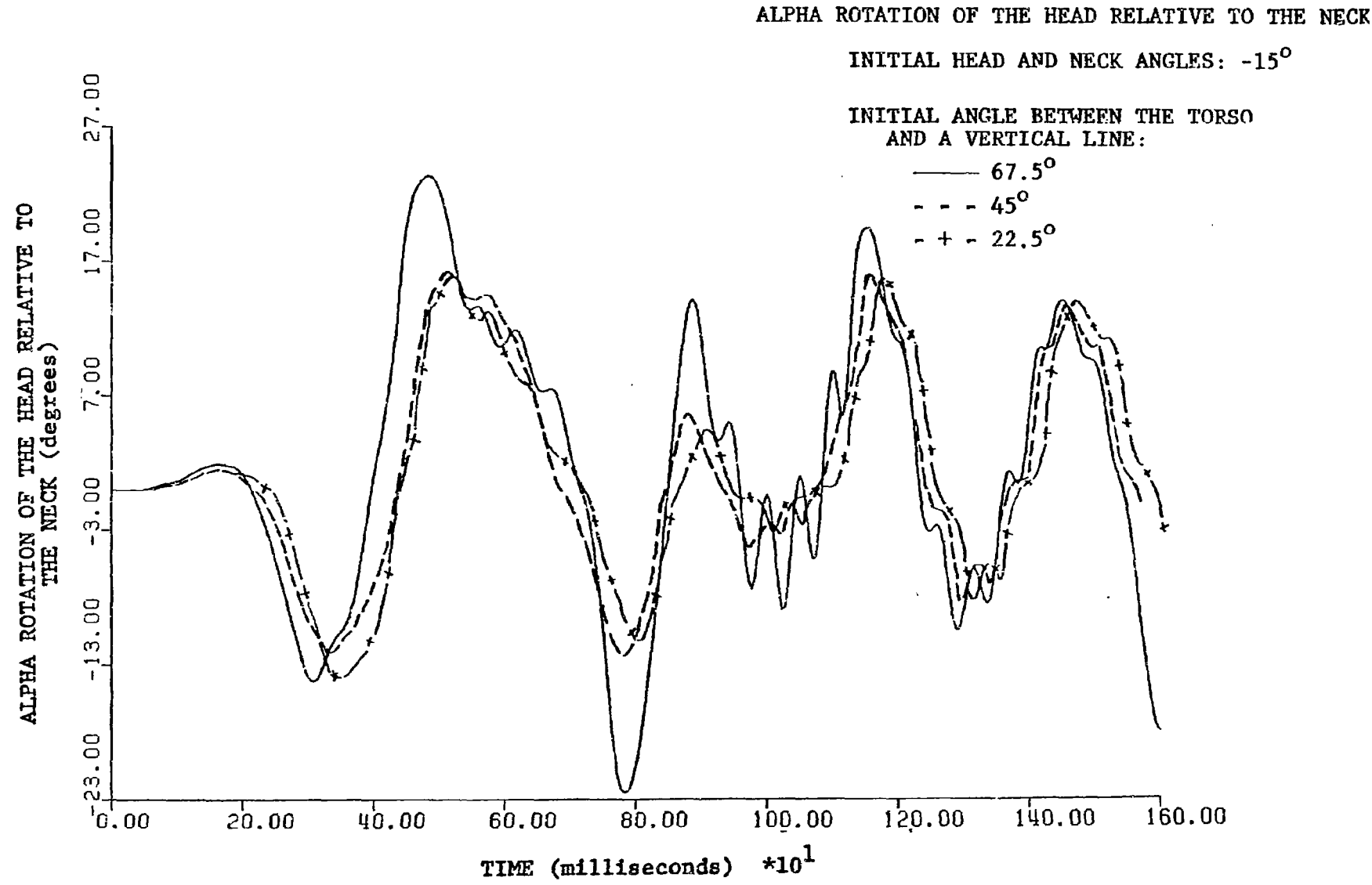

Figure 6. Alpha Rotation of the Head Relative to the Neck

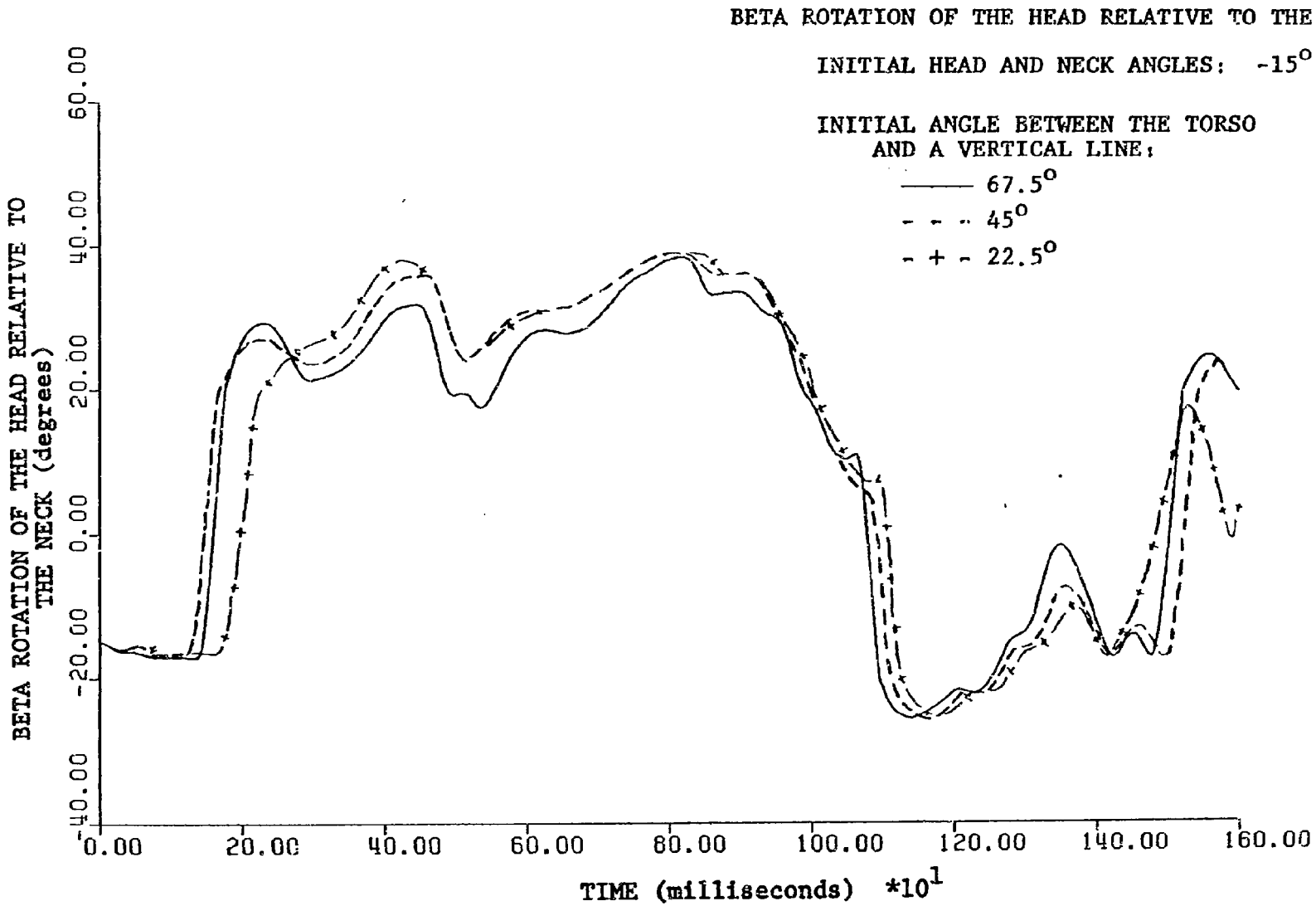

Figure 7. Beta Rotation of the Head Relative to the Neck

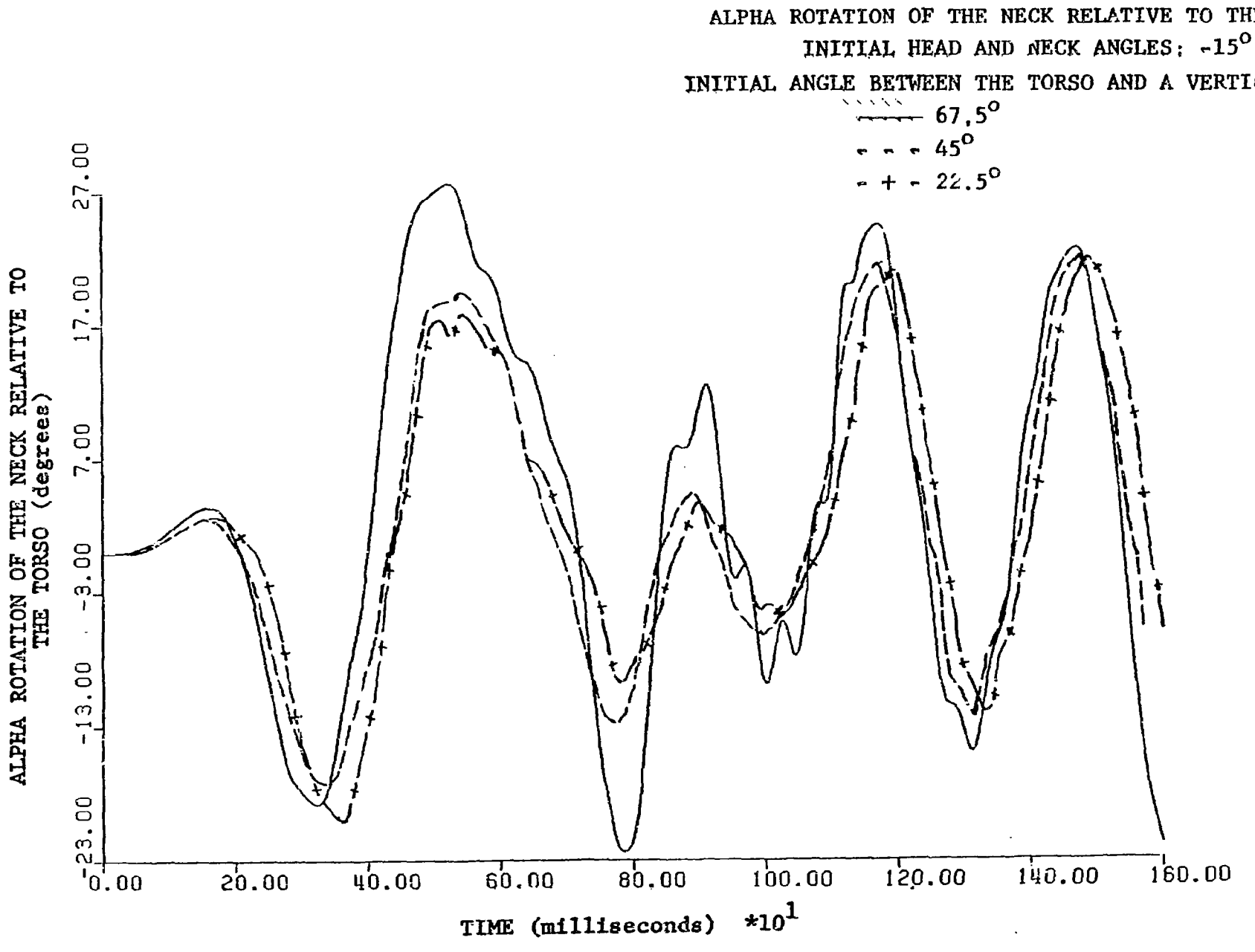

Figure 8. Alpha Rotation of the Neck Relative to the Torso

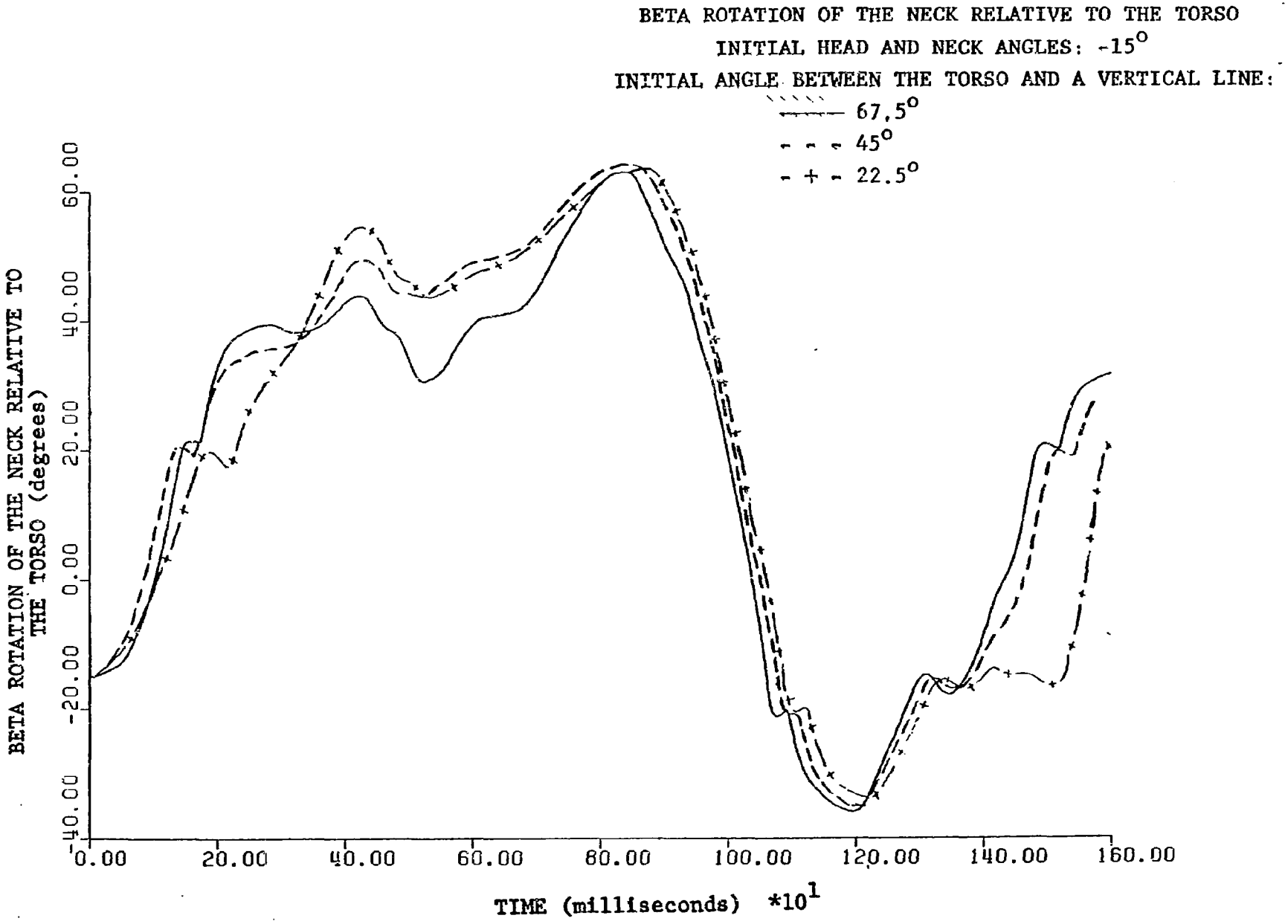

Figure 9. Beta Rotation of the Neck Relative to the Torso

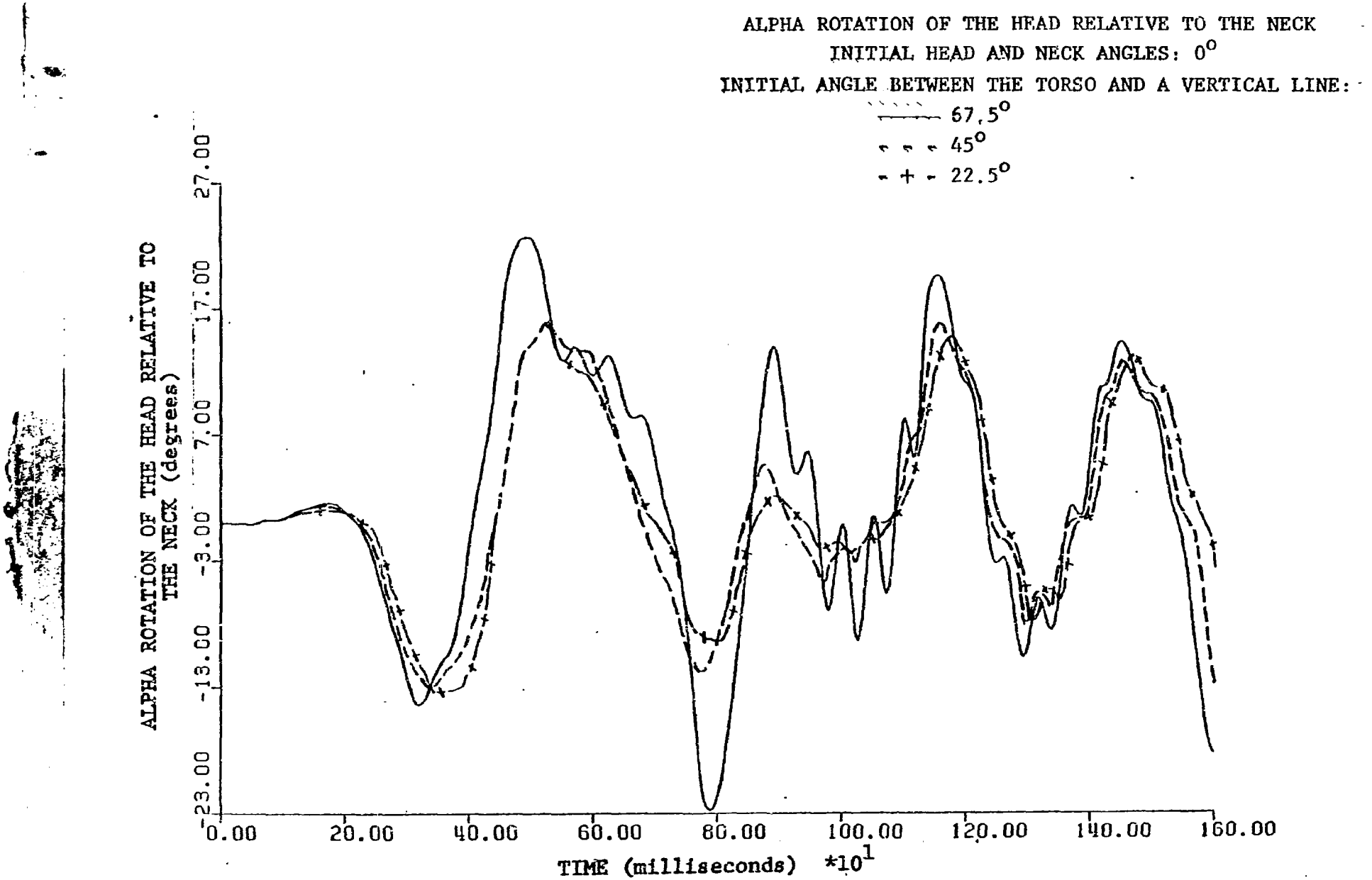

Figure 10. Alpha Rotation of the Head Relative to the Neck

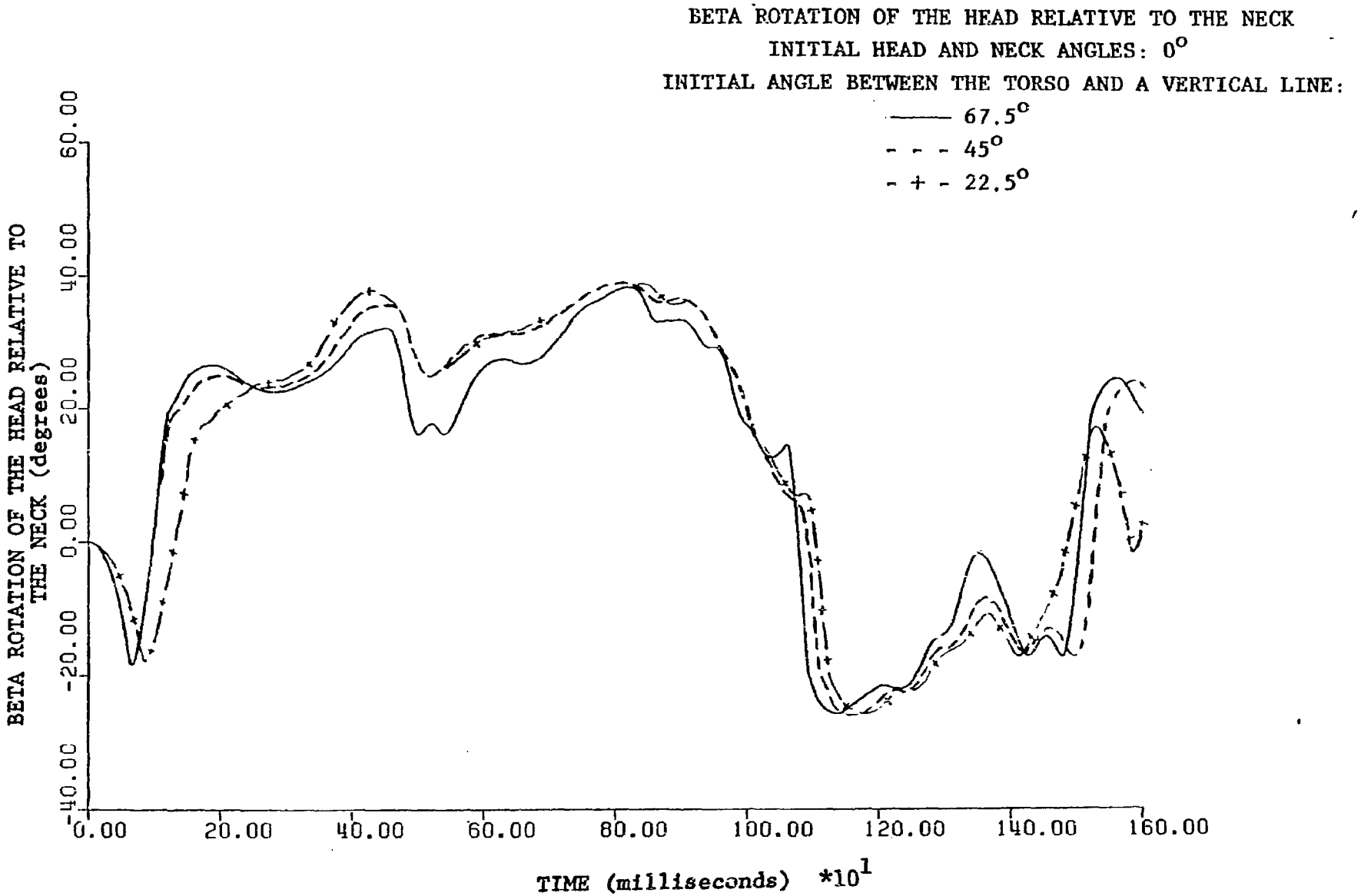

Figure 11. Beta Rotation of the Head Relative to the Neck

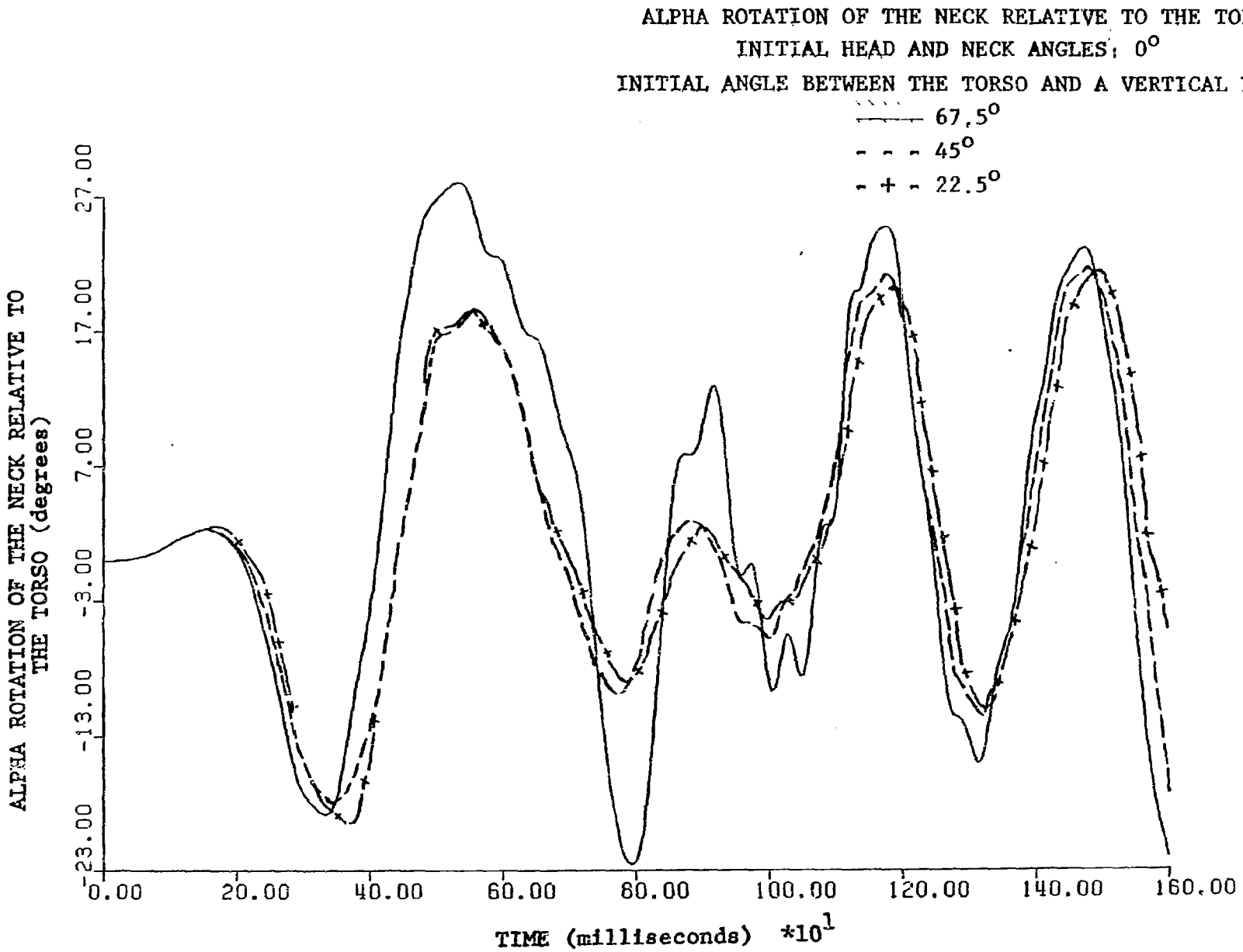

Figure 12. Alpha Rotation of the Neck Relative to the Torso

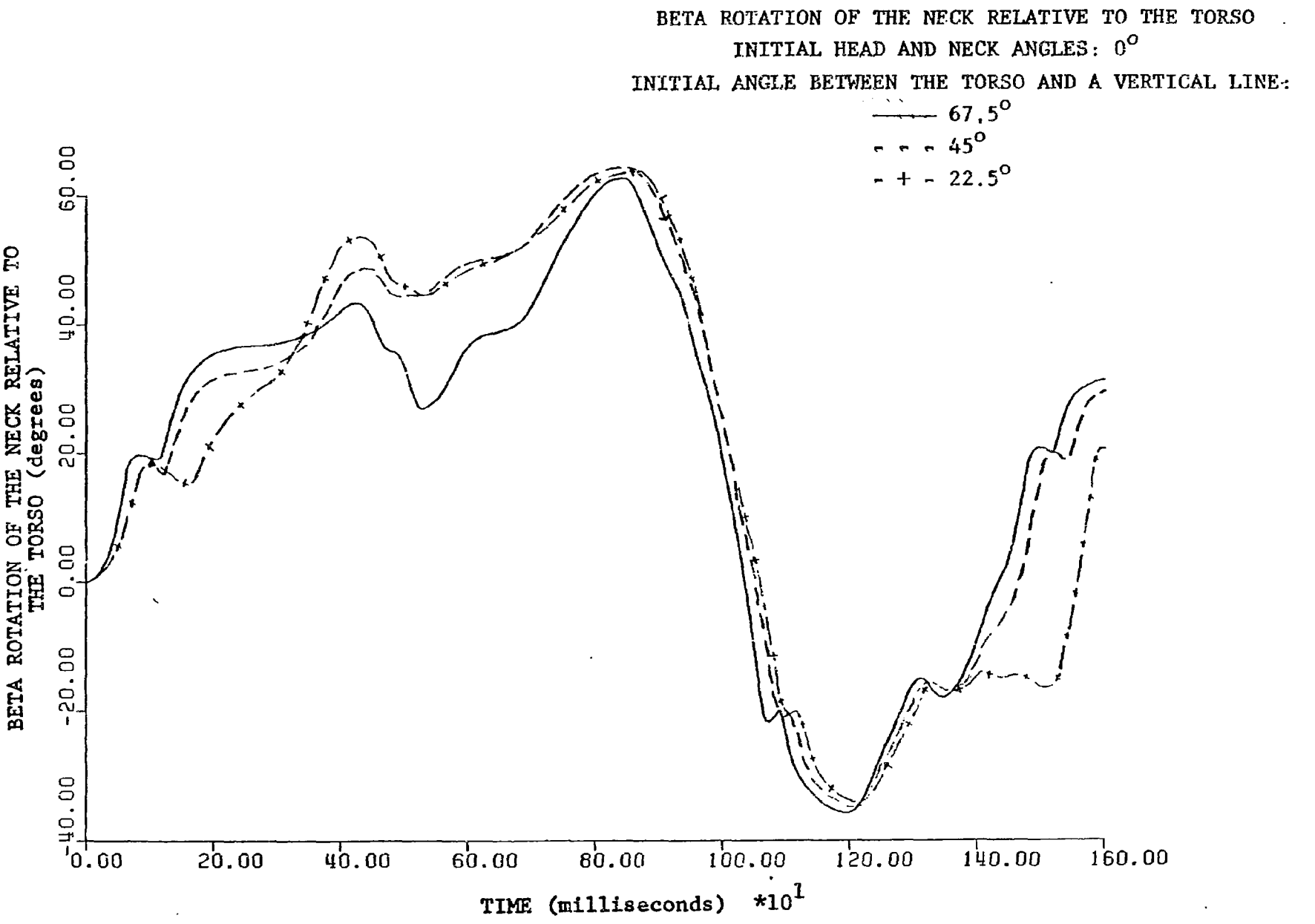

Figure 13. Beta Rotation of the Neck Relative to the Torso

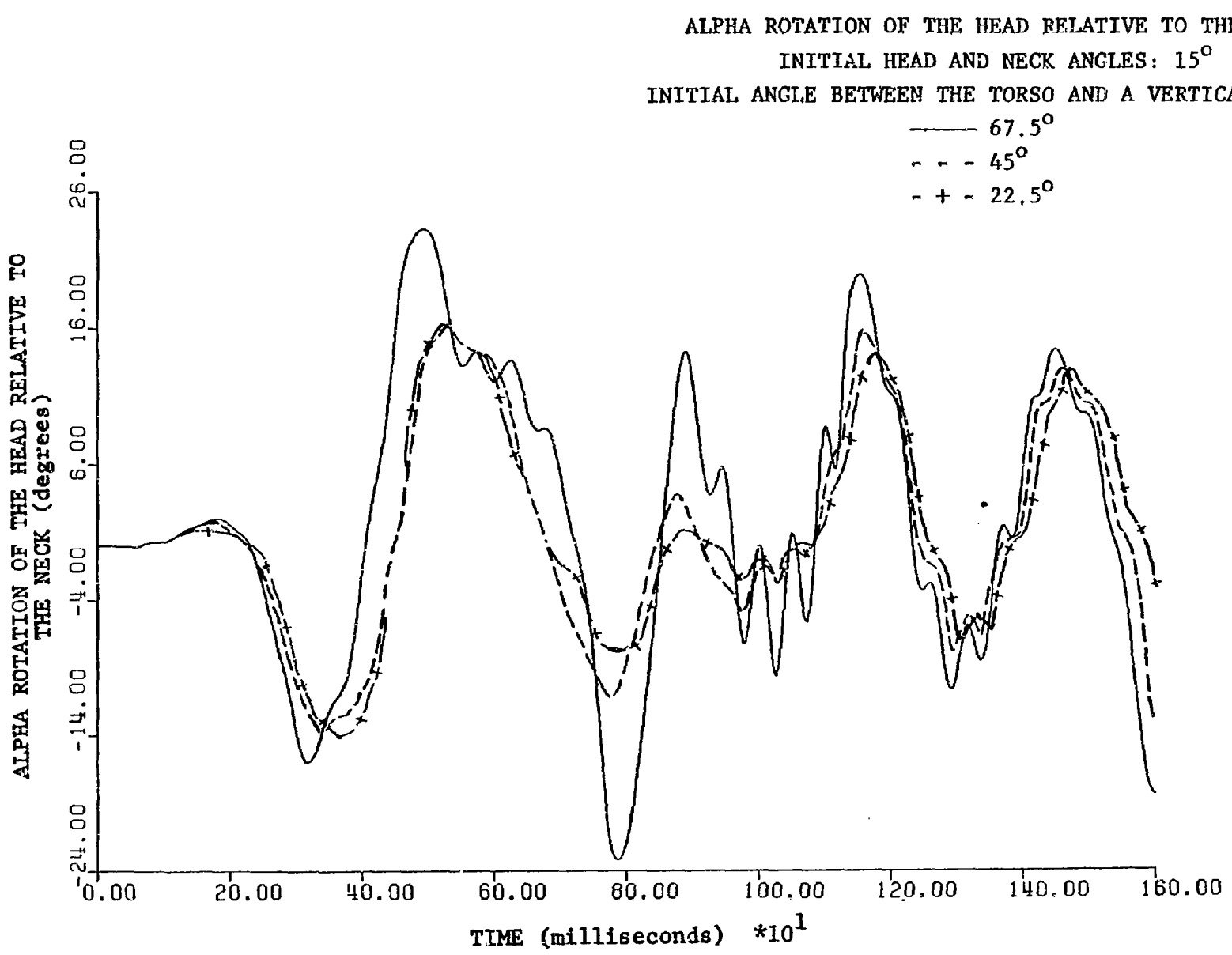

Figure 14. Alpha Rotation of the Head Relative to the Neck

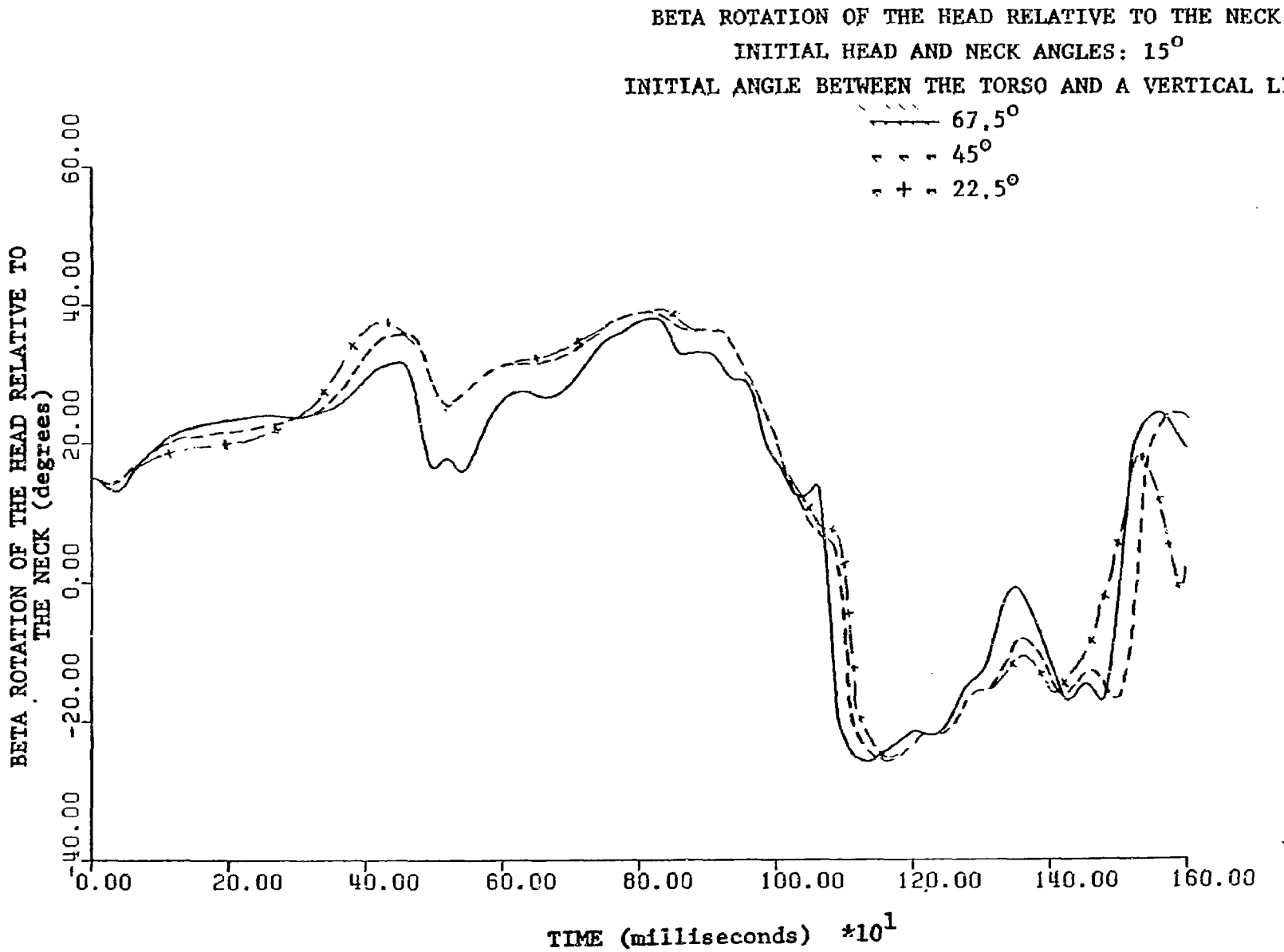

Figure 15, Beta Rotation of the Head Relative to the Neck

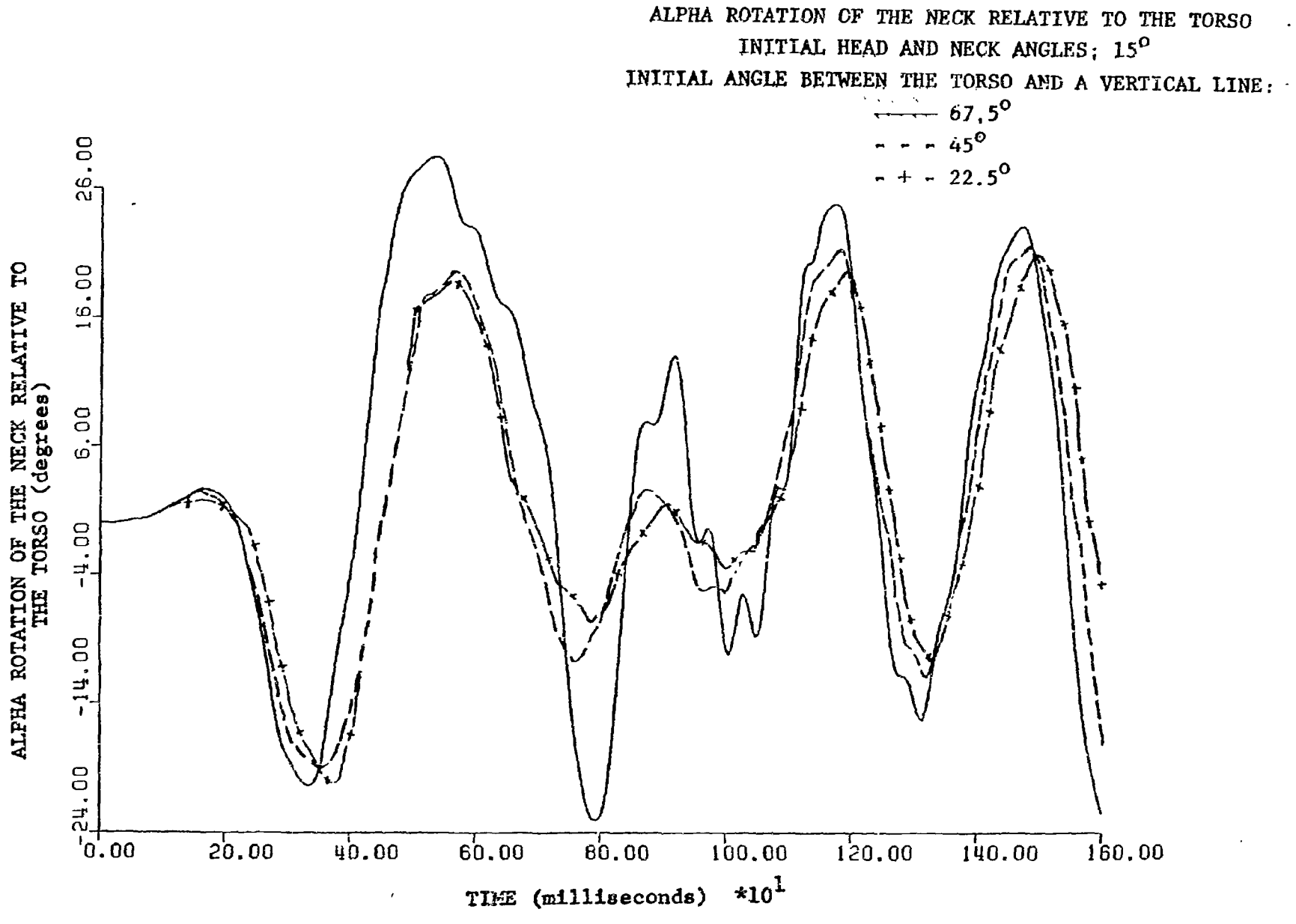

Figure 16. Alpha Rotation of the Neck Relative to the Torso

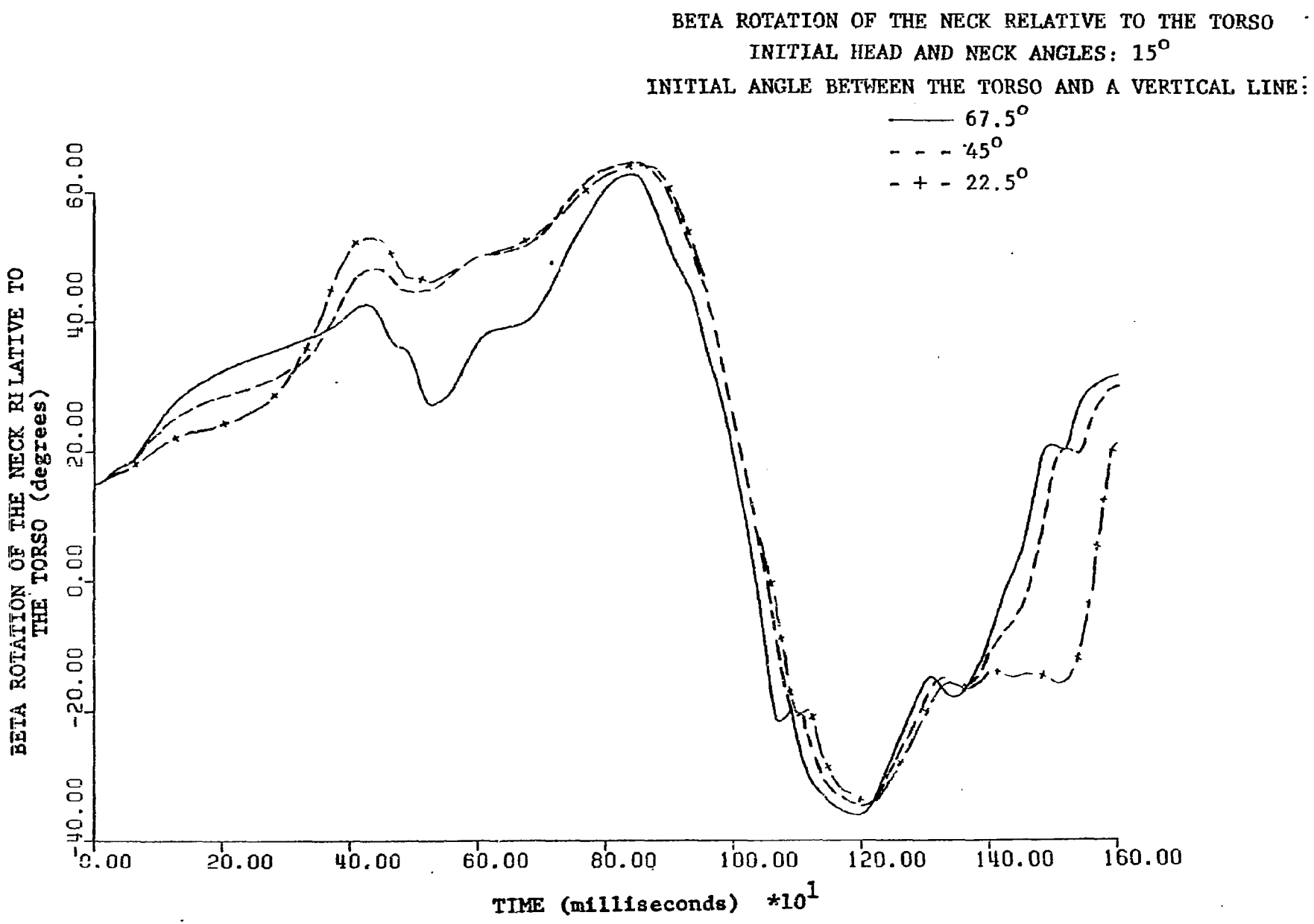

Figure 17. Beta Rotation of the Neck Relative to the Torso

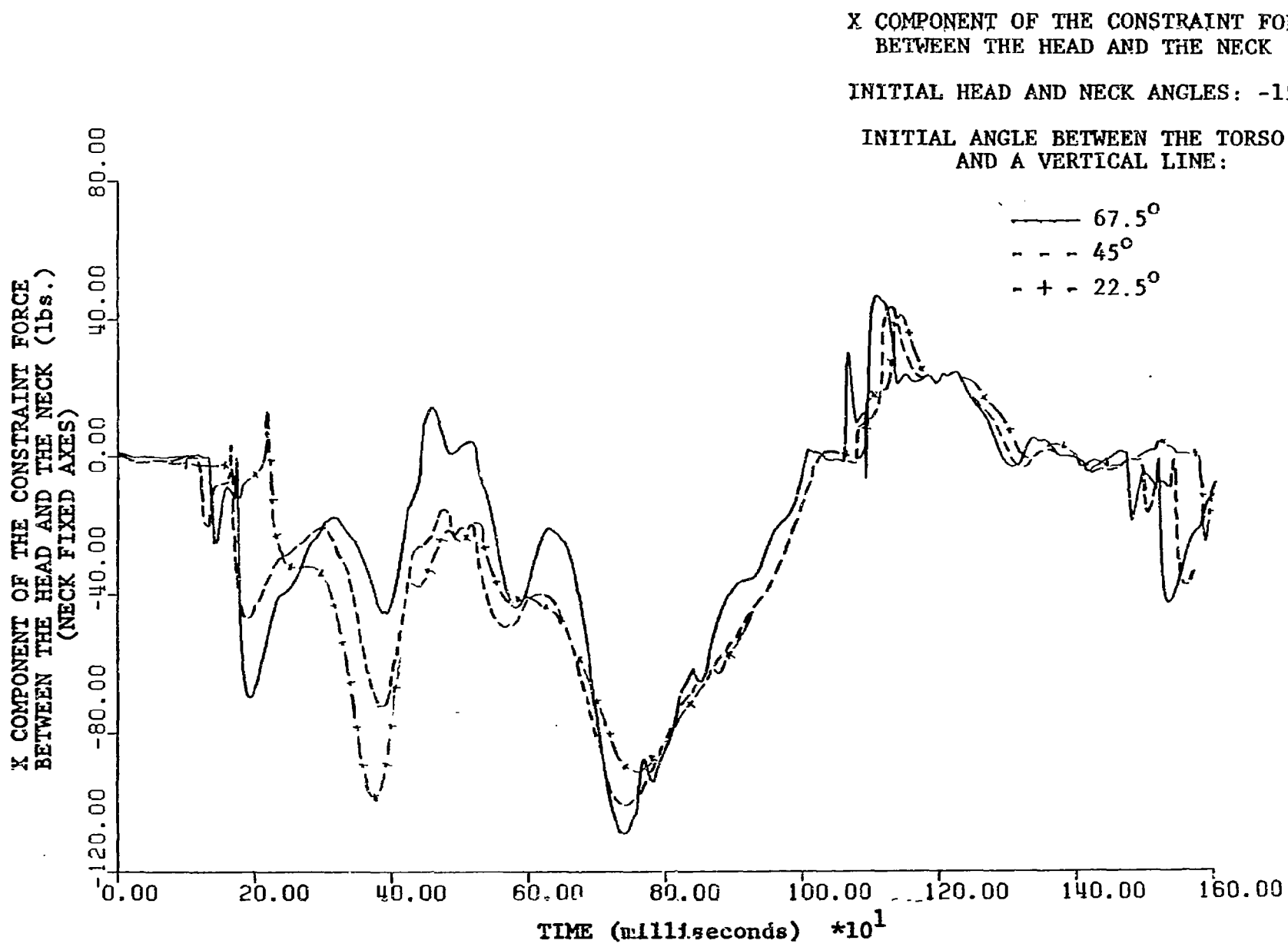

Figure 18. X Component of the Constraint Force Between the Head and the Neck

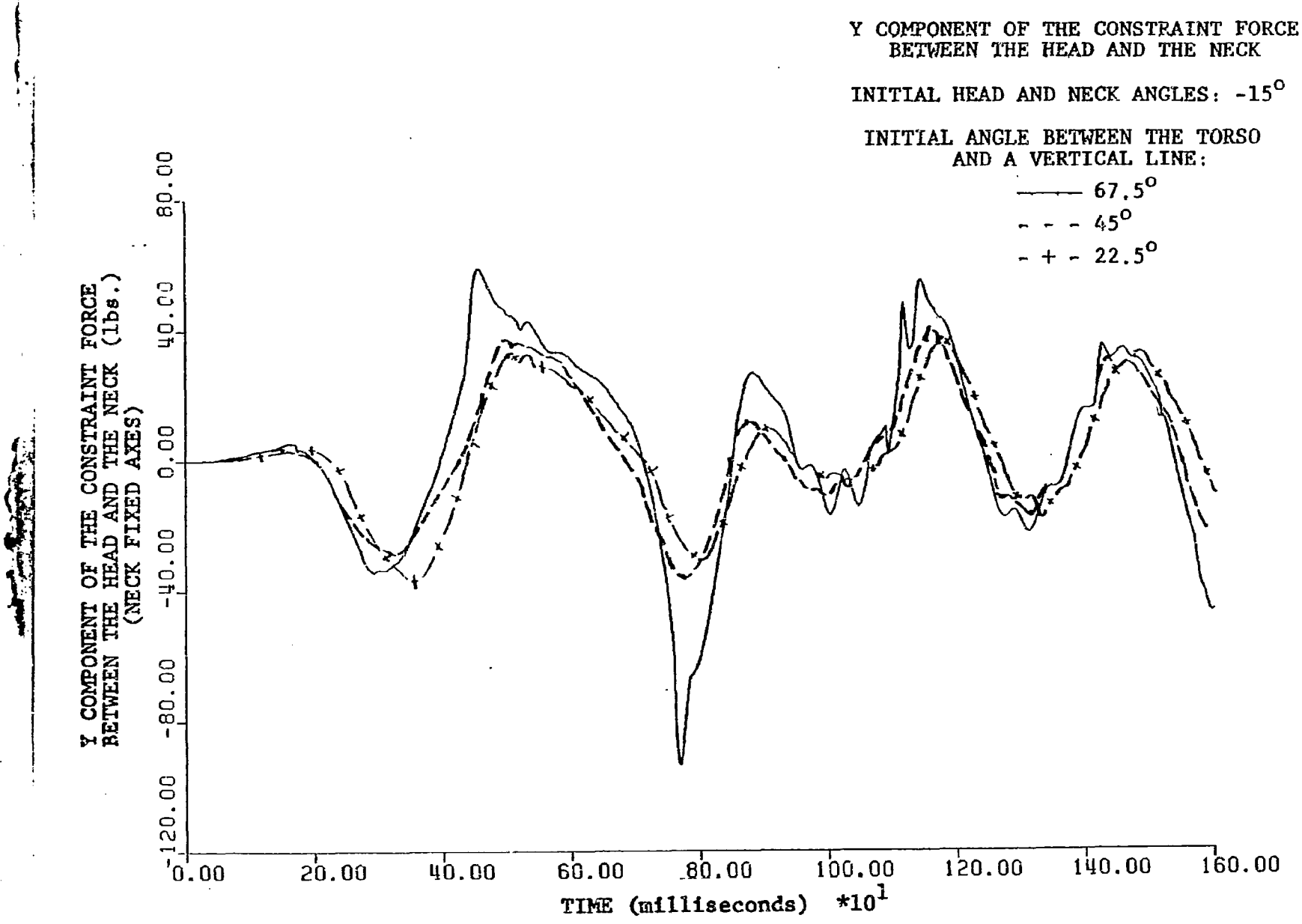

Figure 19, Y Component of the Constraint Force Between the Head and the Neck

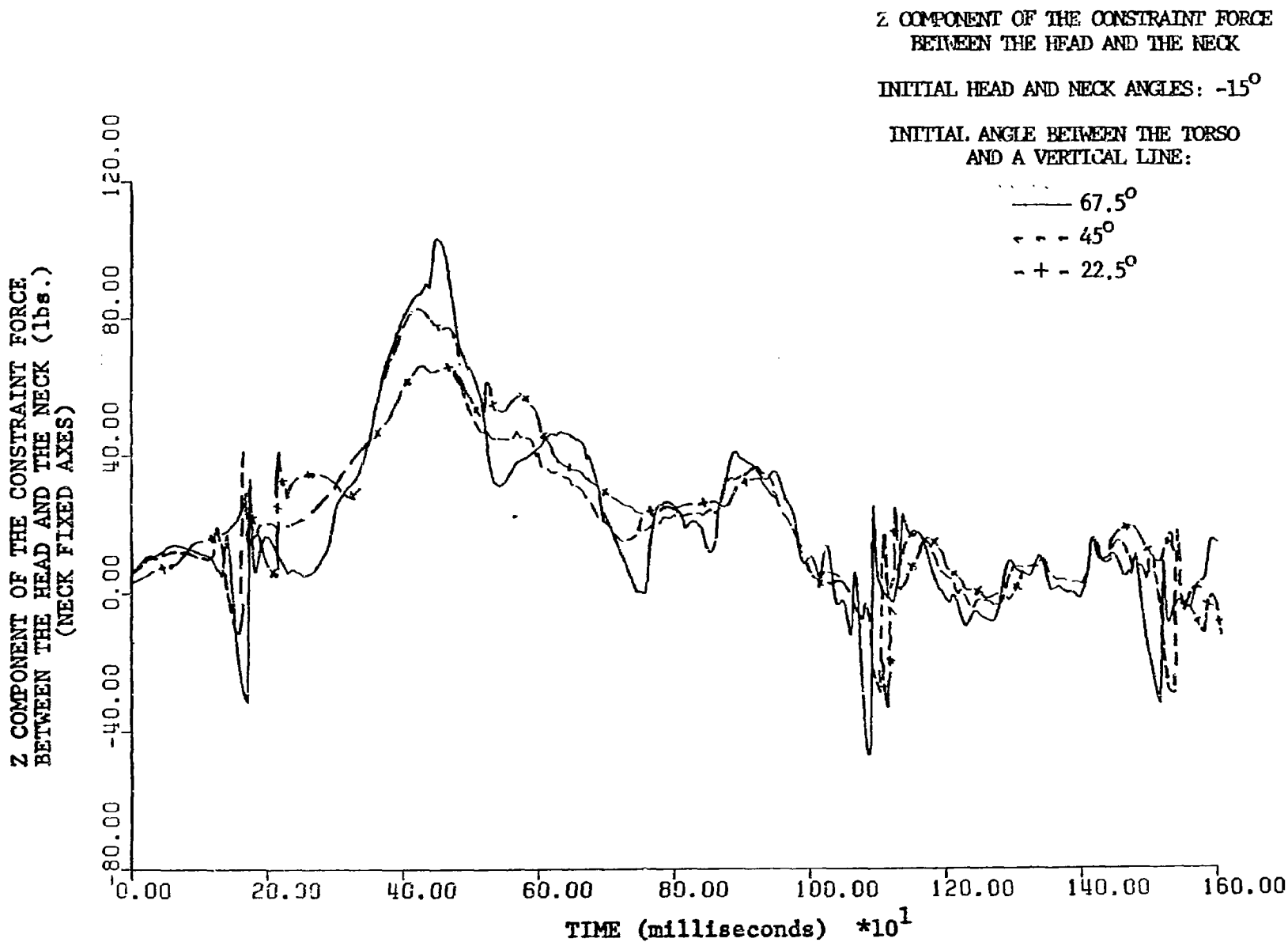

Figure 20. Z Component of the Constraint Force Between the Head and the Neck

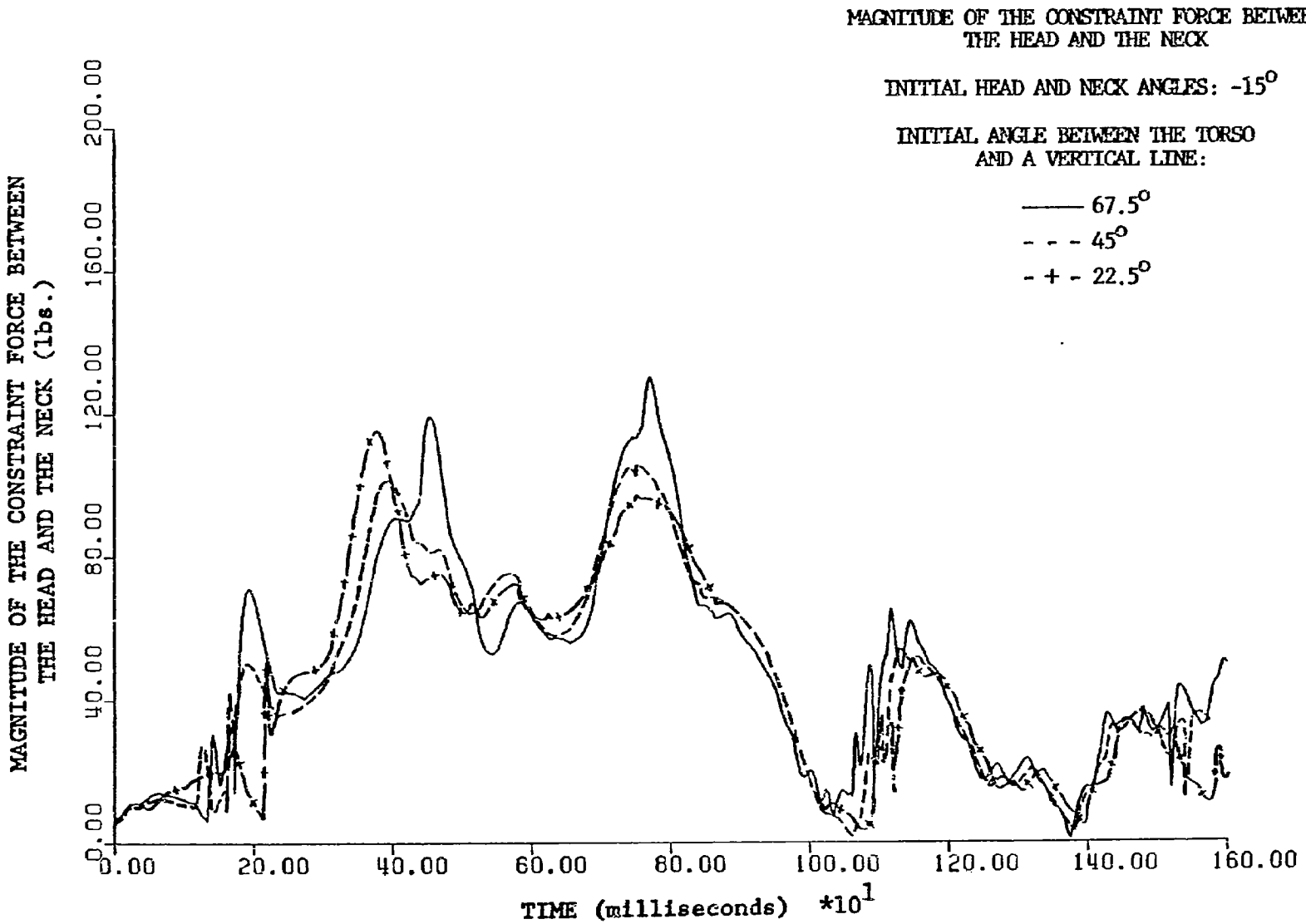

Figure 21. Magnitude of the Constraint Force Between the Head and the Neck

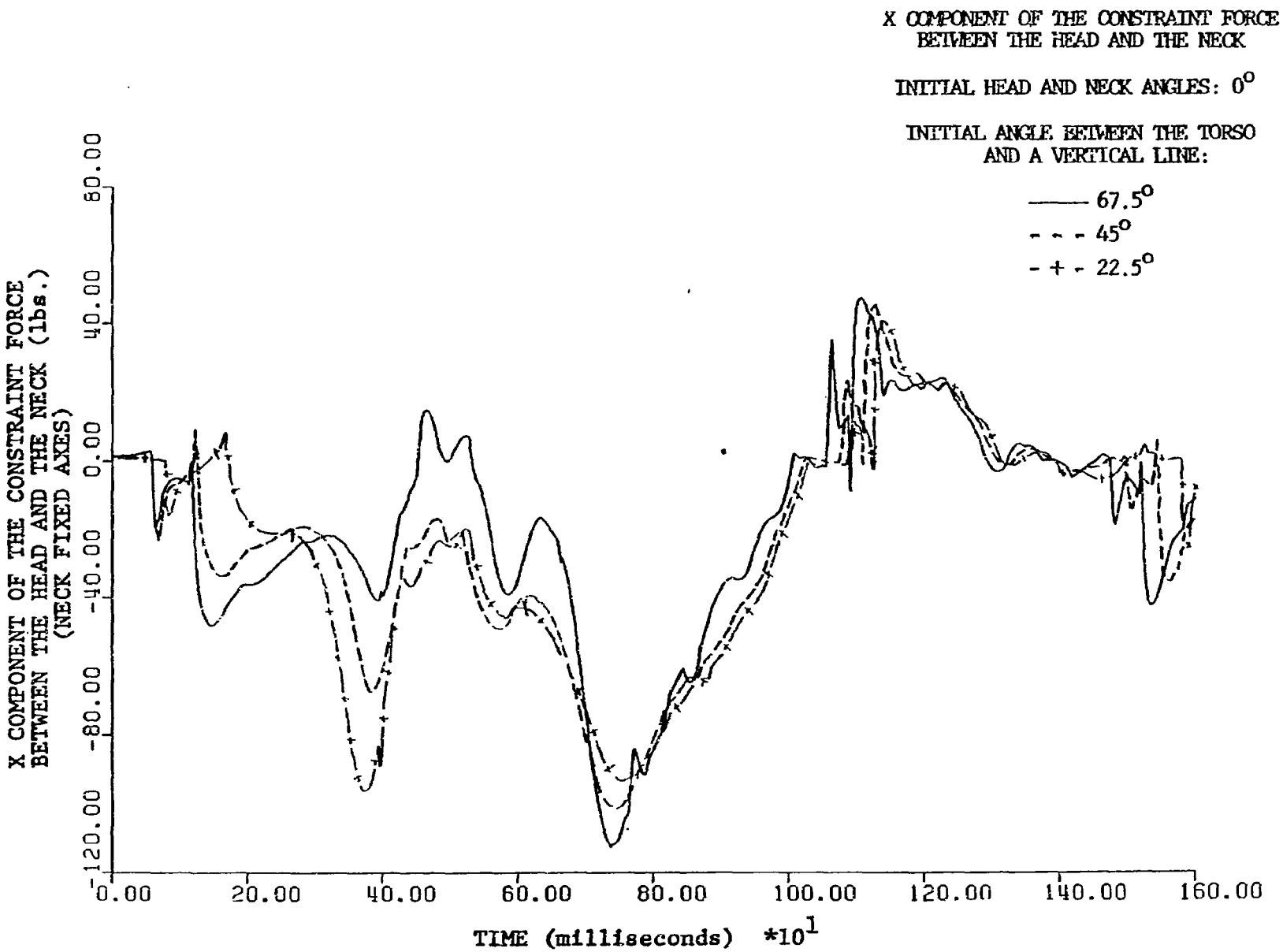

Figure 22. X Component of the Constraint Force Between the Head and the Neck

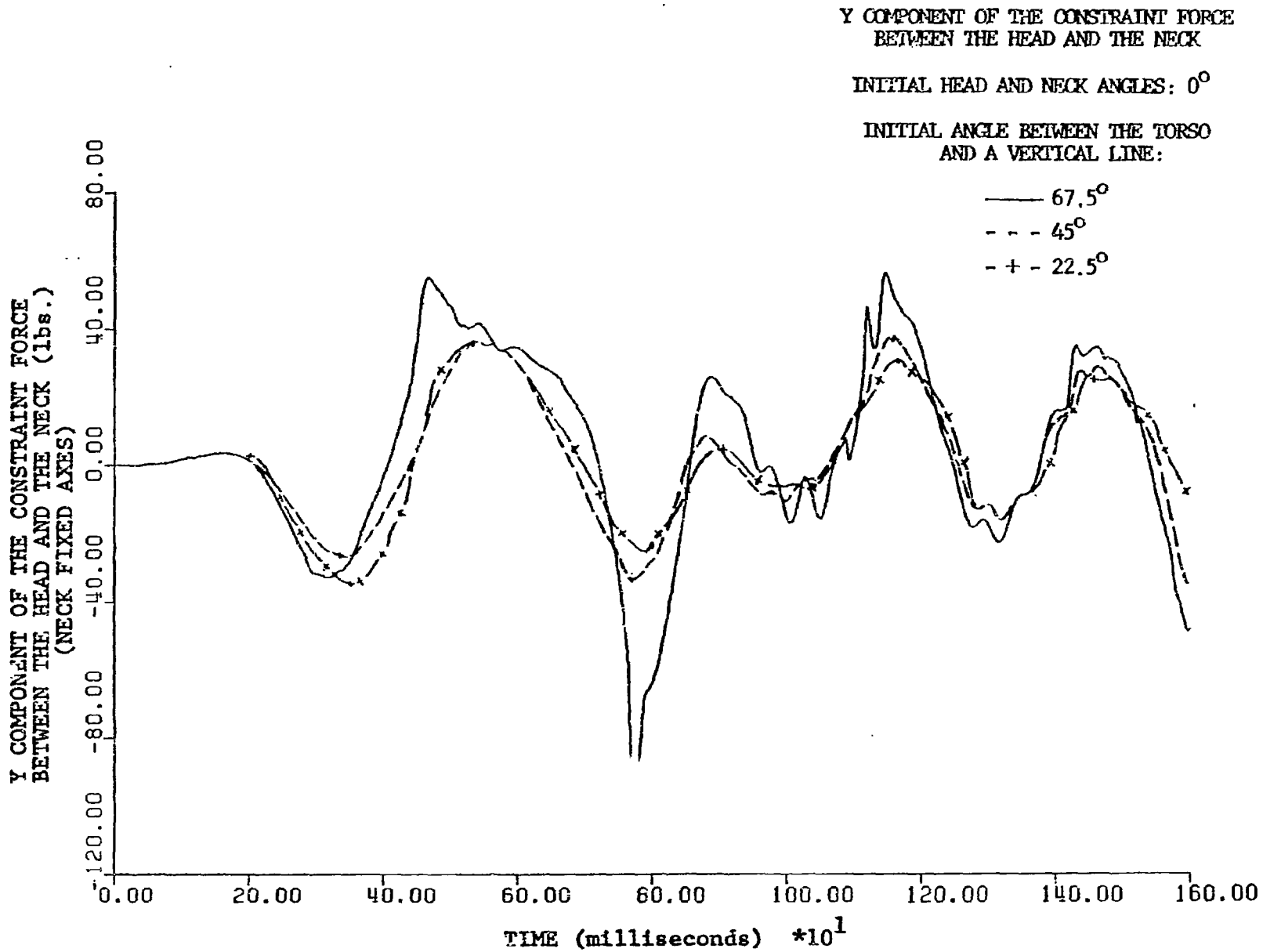

Figure 23. Y Component of the Constraint Force Between the Head and the Neck

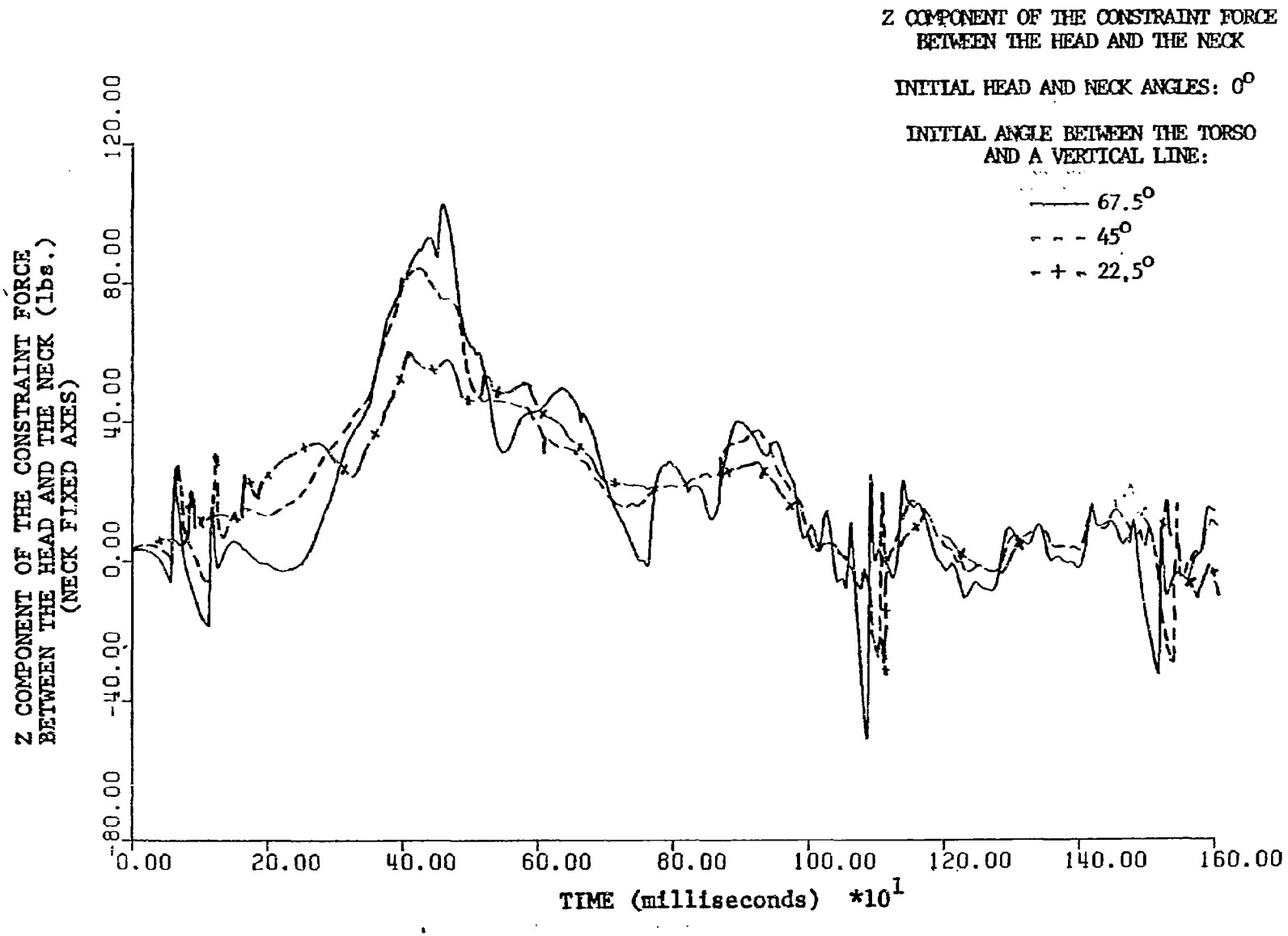

Figure 24. Z Component of the Constraint Force Between the Head and Neck

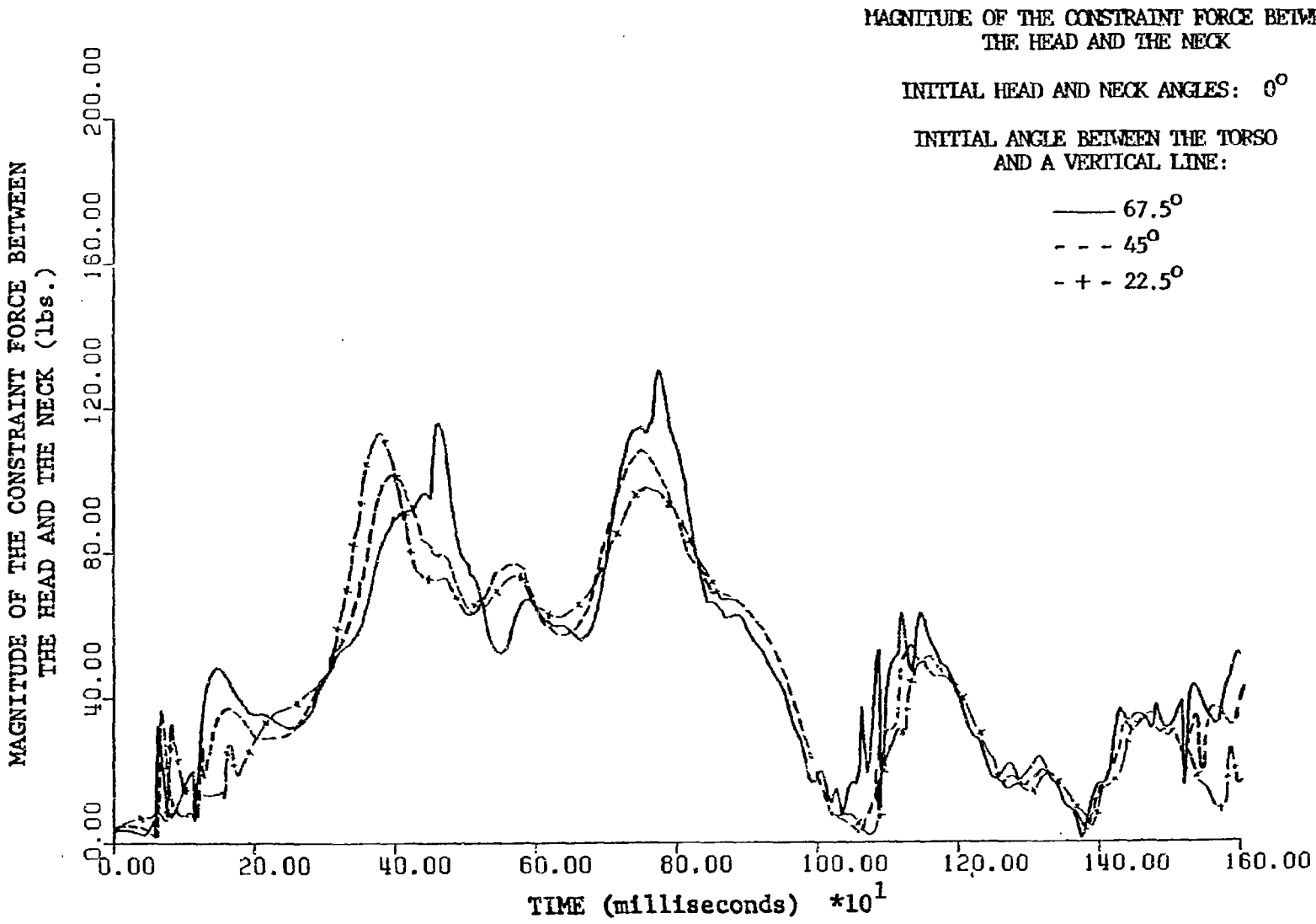

Figure 25. Magnitude of the Constraint Force Between the Head and the Neck

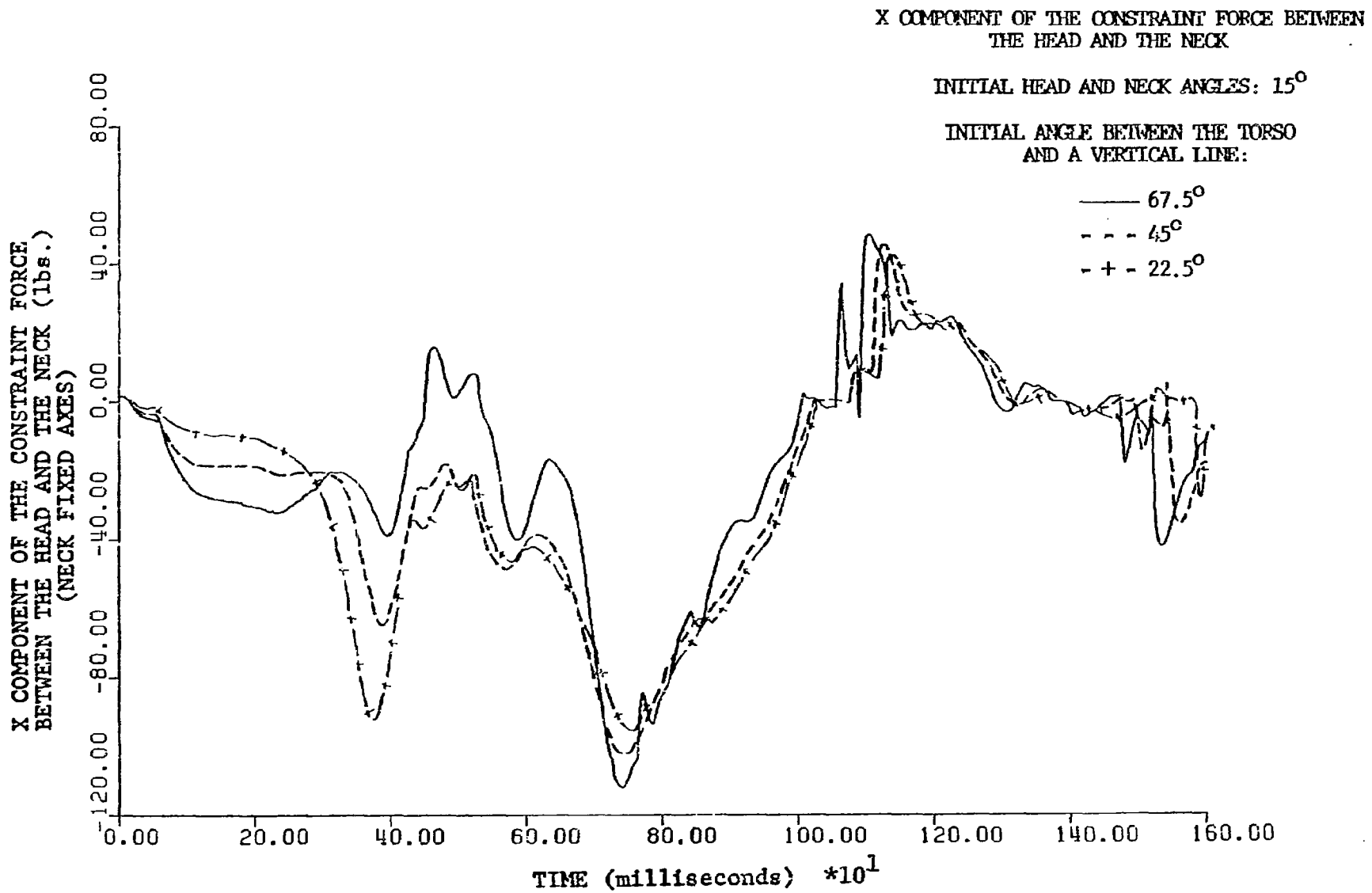

Figure 26. X Component of the Constraint Force Between the Head and the Neck

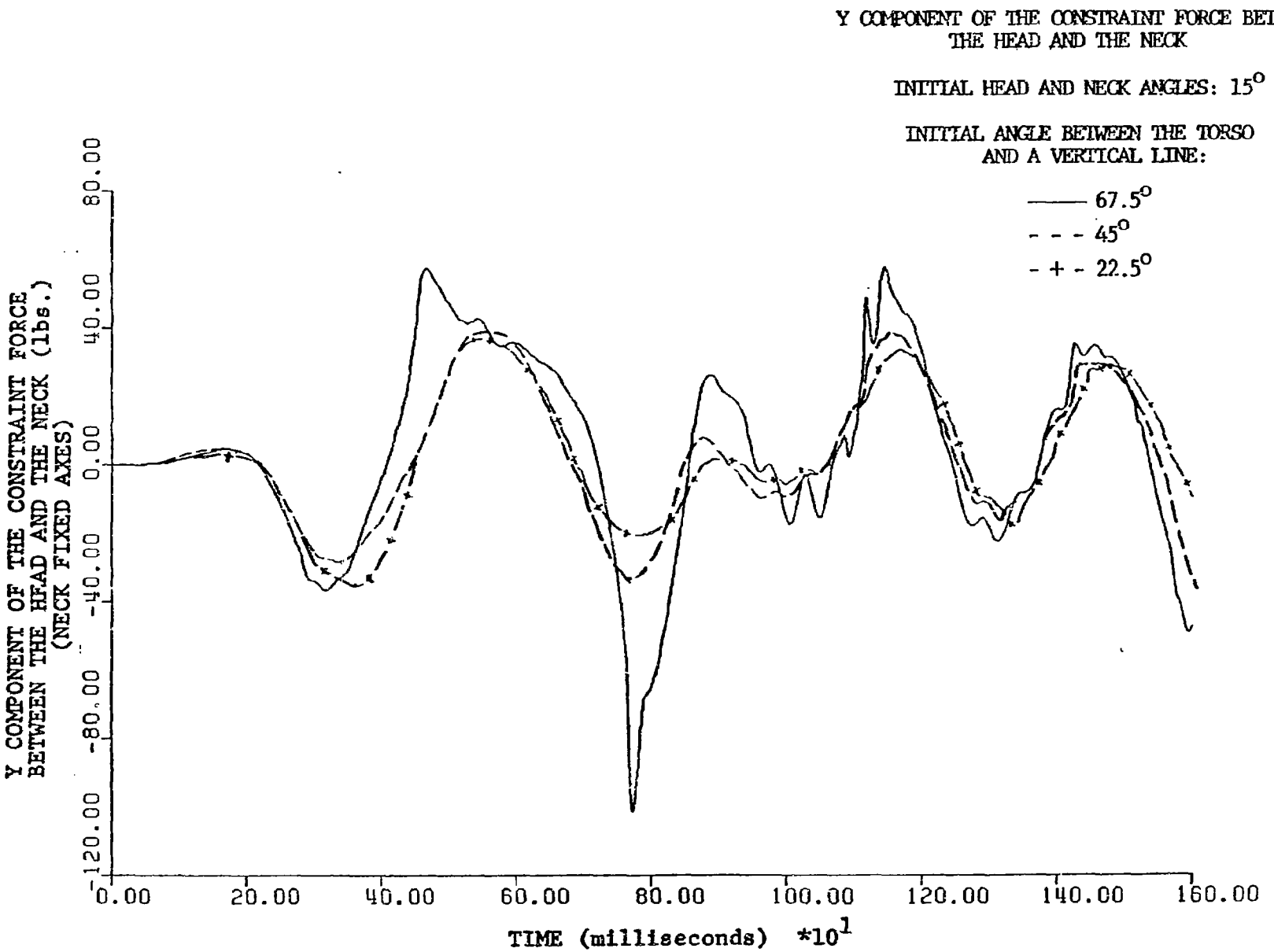

Figure 27. Y Component of the Constraint Force Between the Head and the Neck

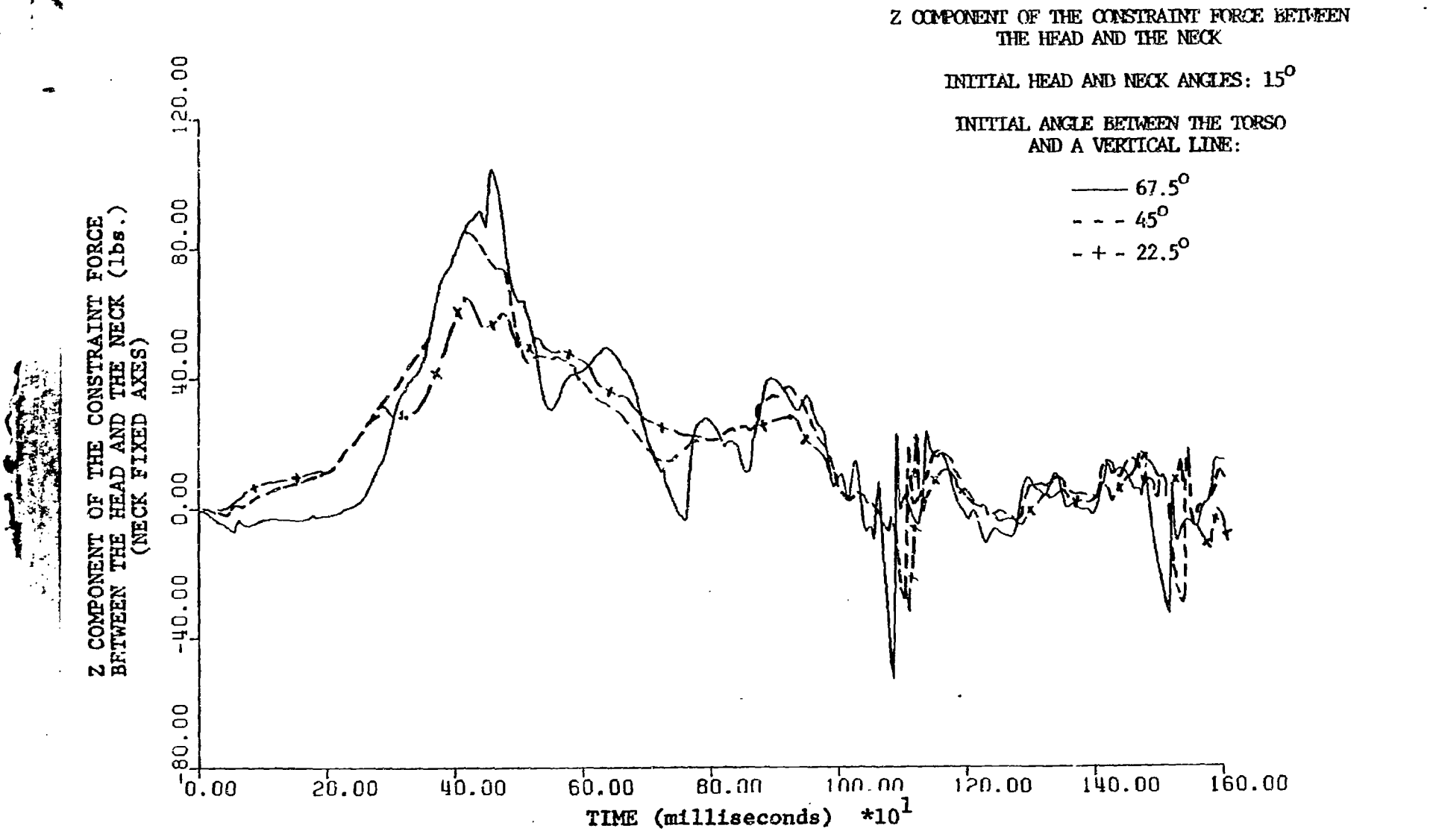

Figure 28. Z Component of the Constraint Force Between the Head and the Neck

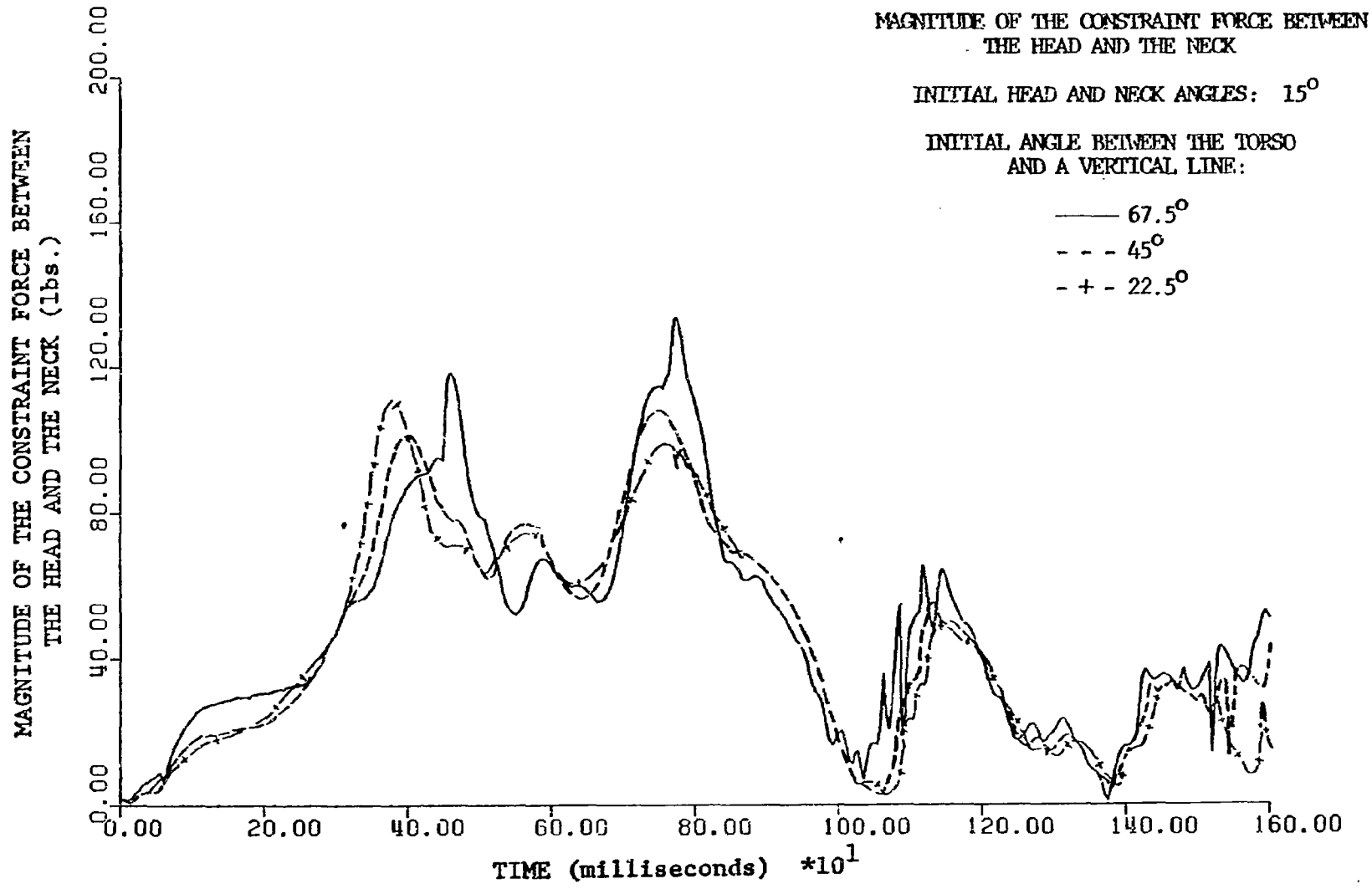

Figure 29. Magnitude of the Constraint Force Between the Head and the Neck

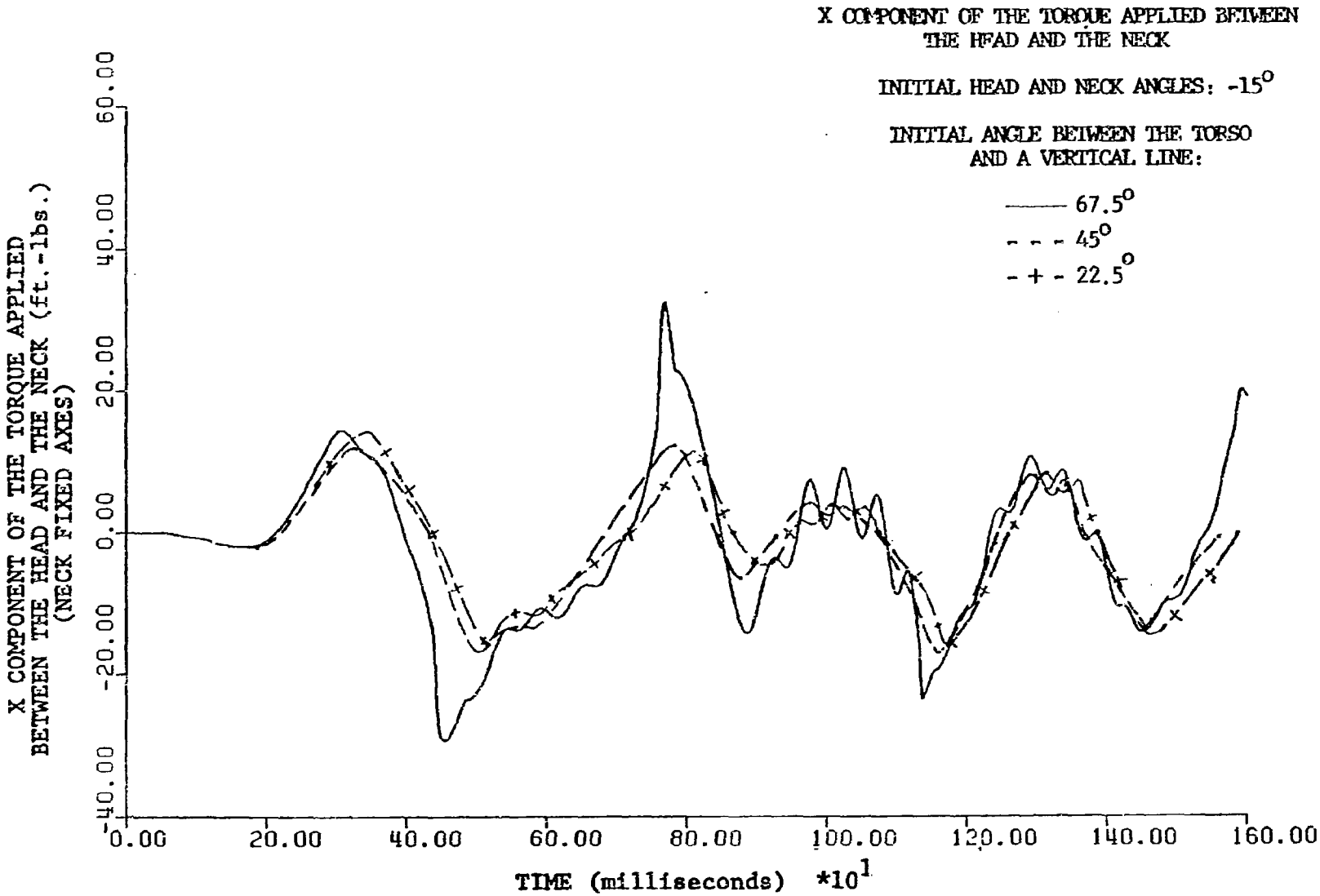

Figure 30. X Component of the Torque Applied Between the Head and the Neck

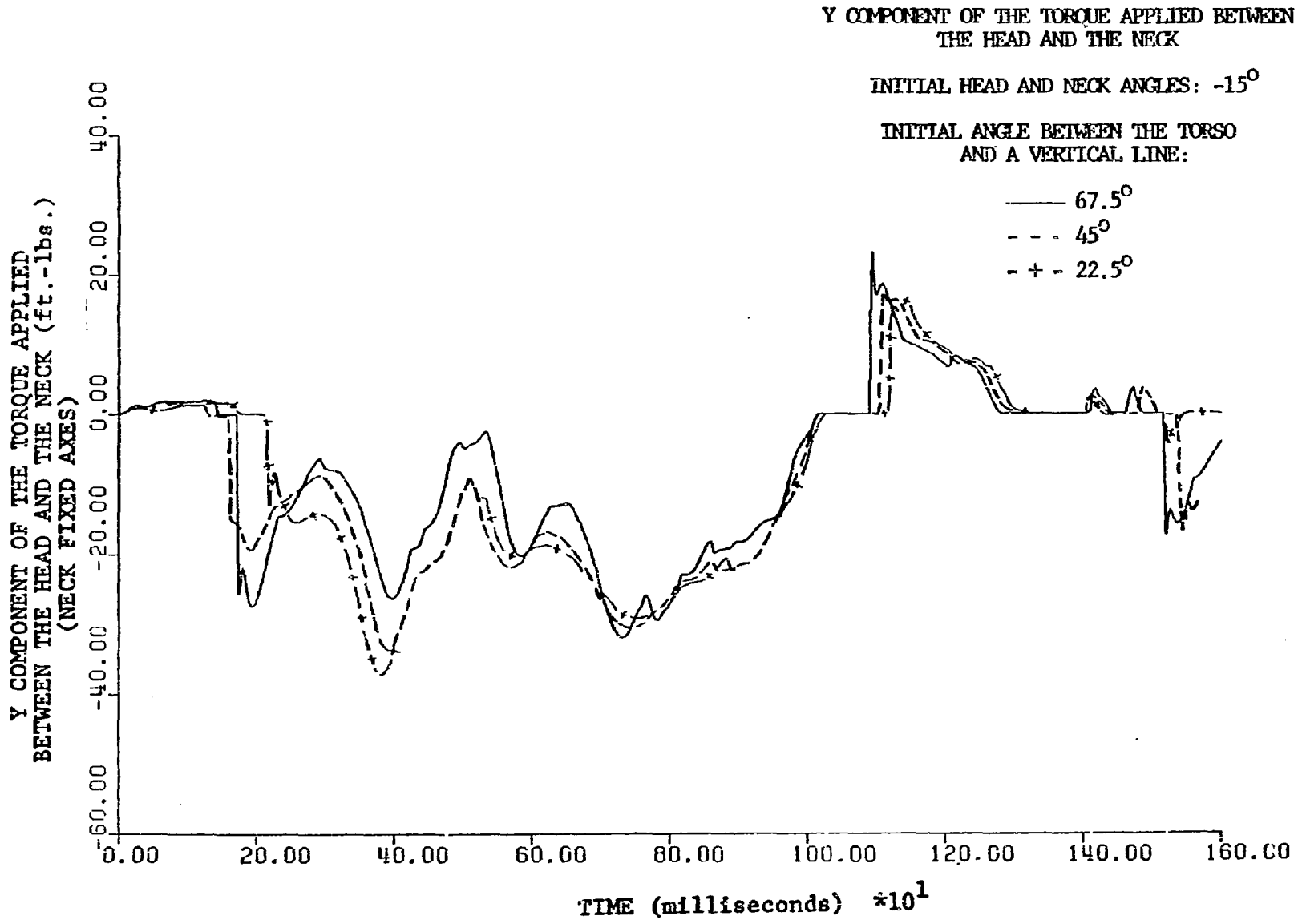

Figure 31. Y Component of the Torque Applied Between the Head and the Neck

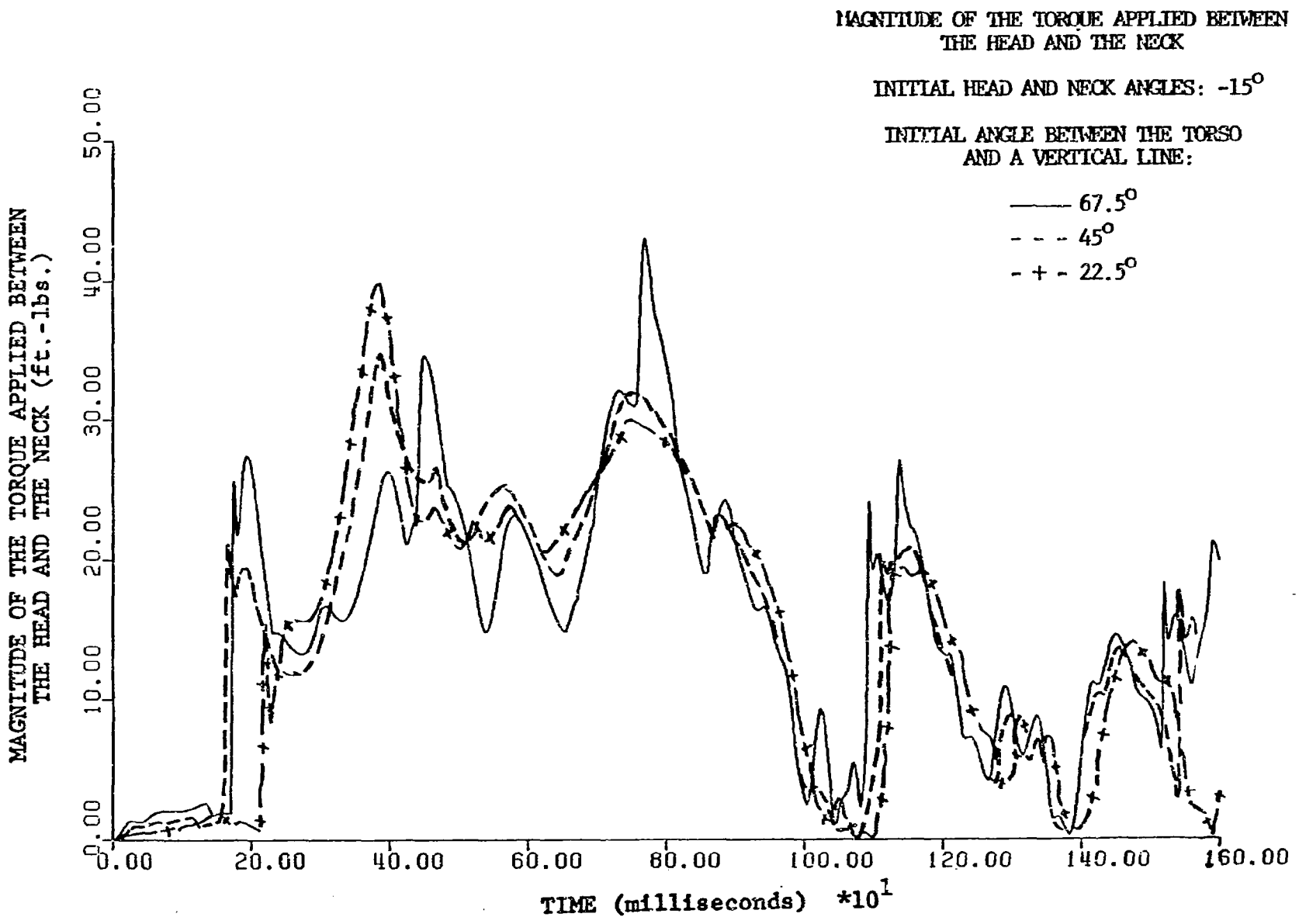

Figure 32. Magnitude of the Torque Applied Between the Head and the Neck

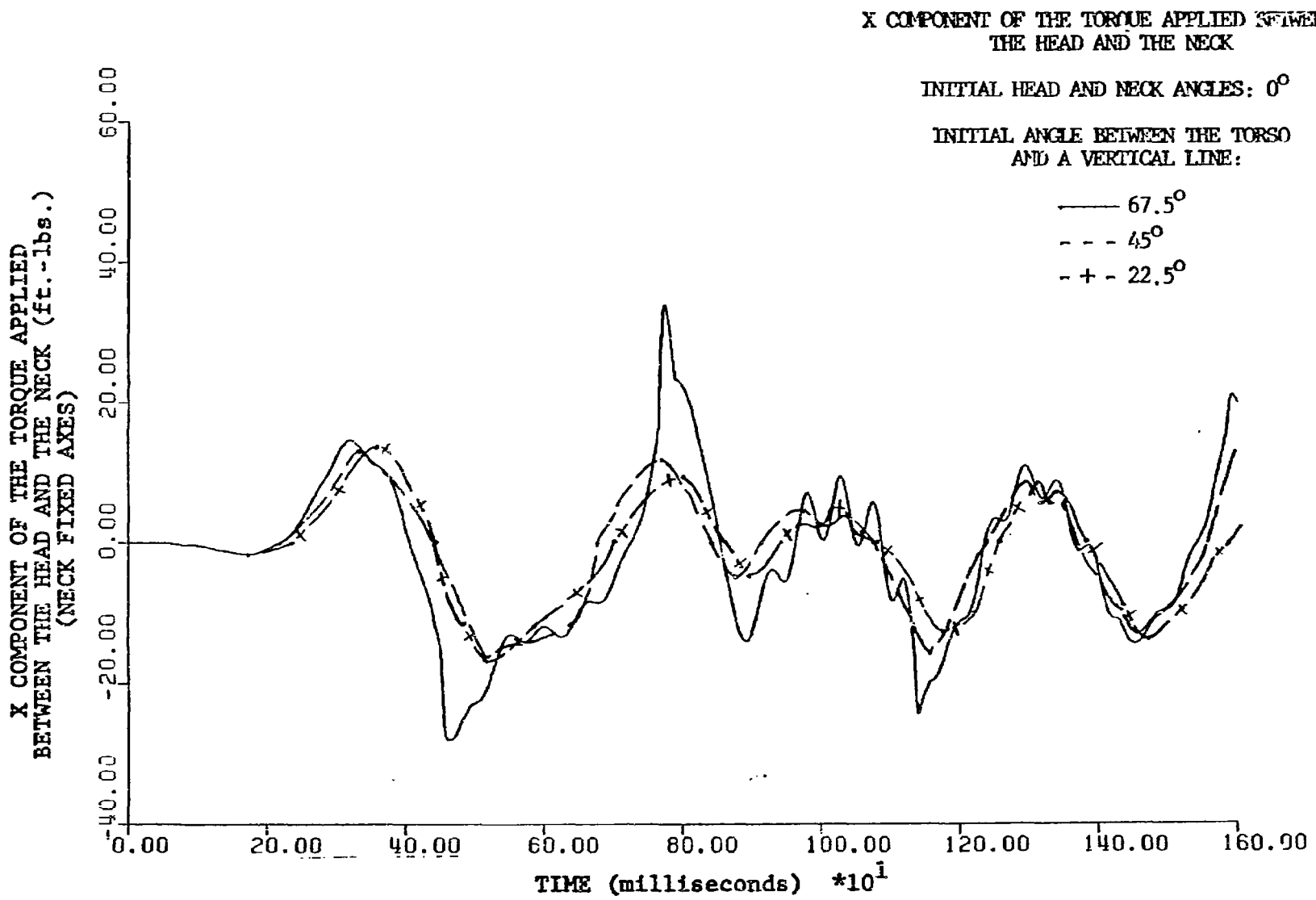

Figure 33. X Component of the Torque Applied Between the Head and the Neck

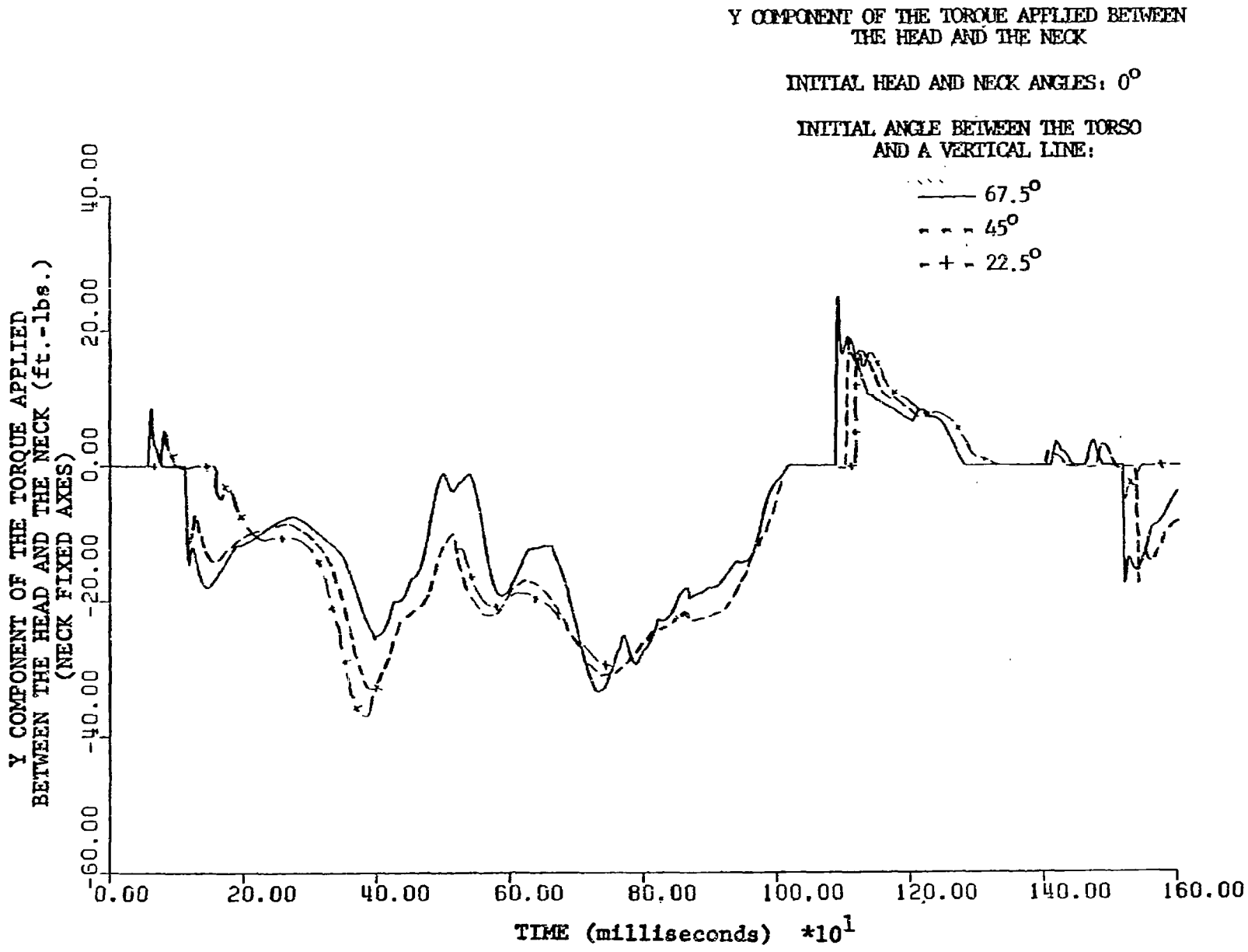

Figure 34. Y Component of the Torque Applied Between the Head and the Neck

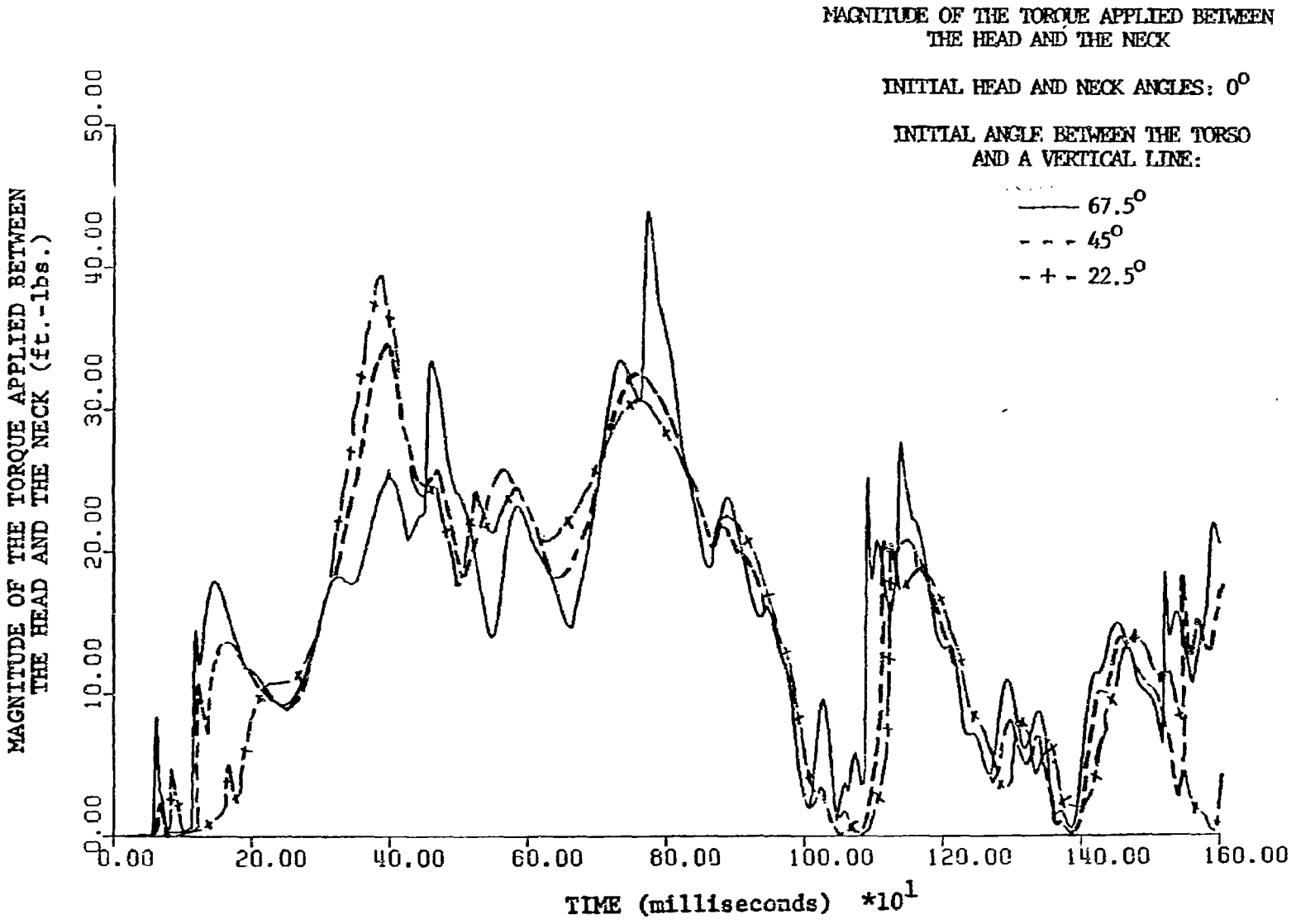

Figure 35, Magnitude of the Torque Applied Between the Head and the Neck

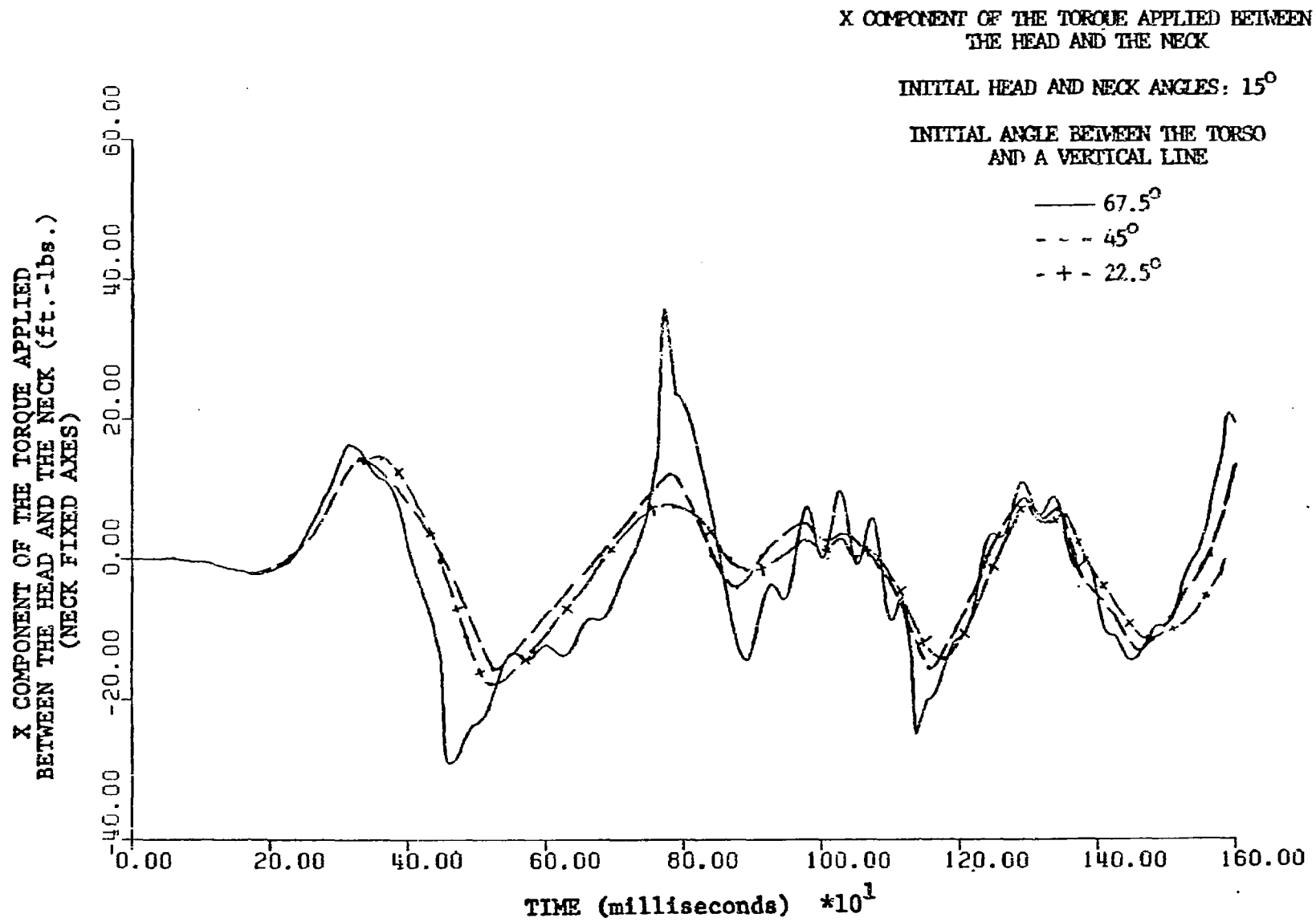

Figure 36. X Component of the Torque Applied Between the Head and the Neck

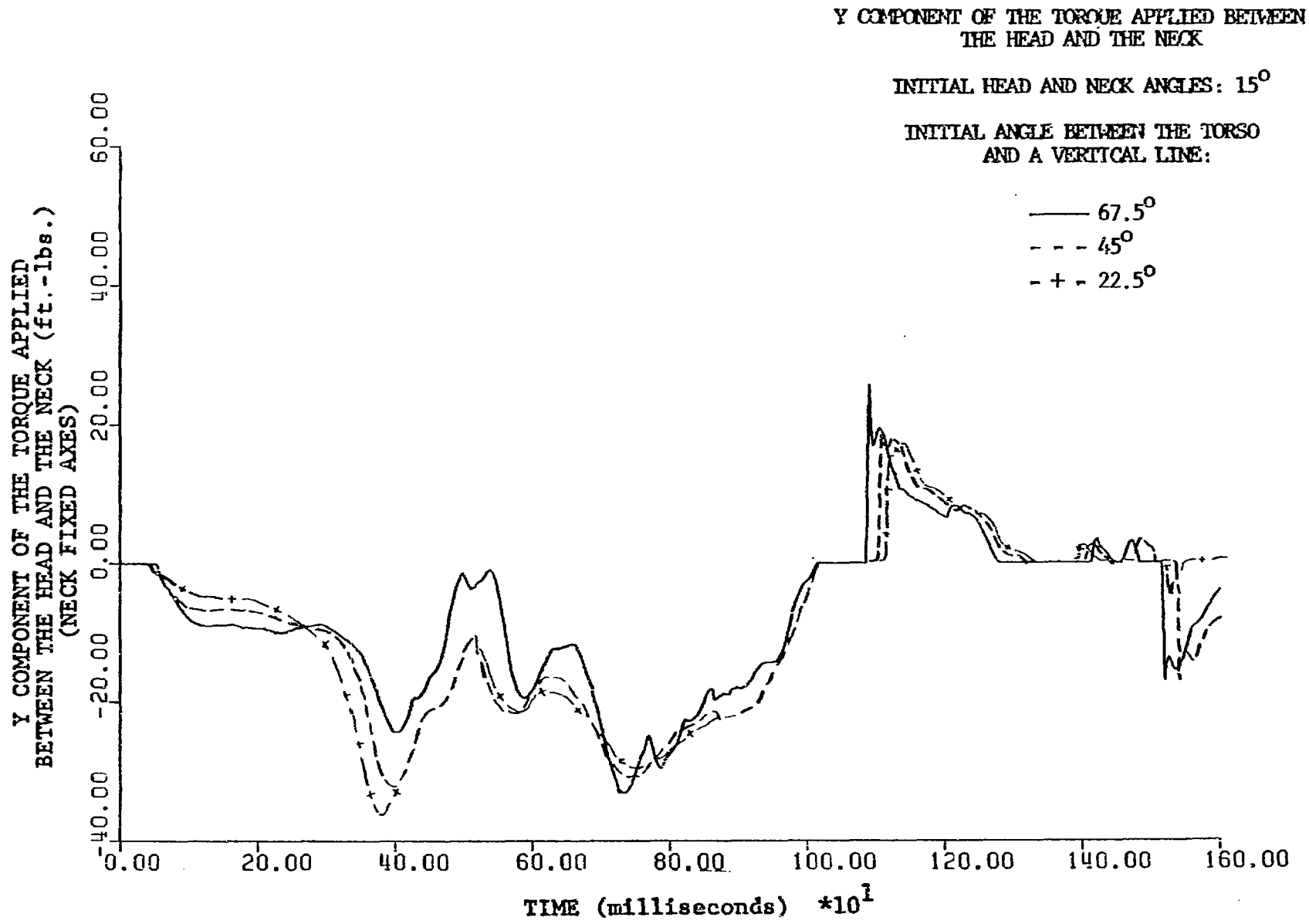

Figure 37. Y Component of the Torque Applied Between the Head and the Neck

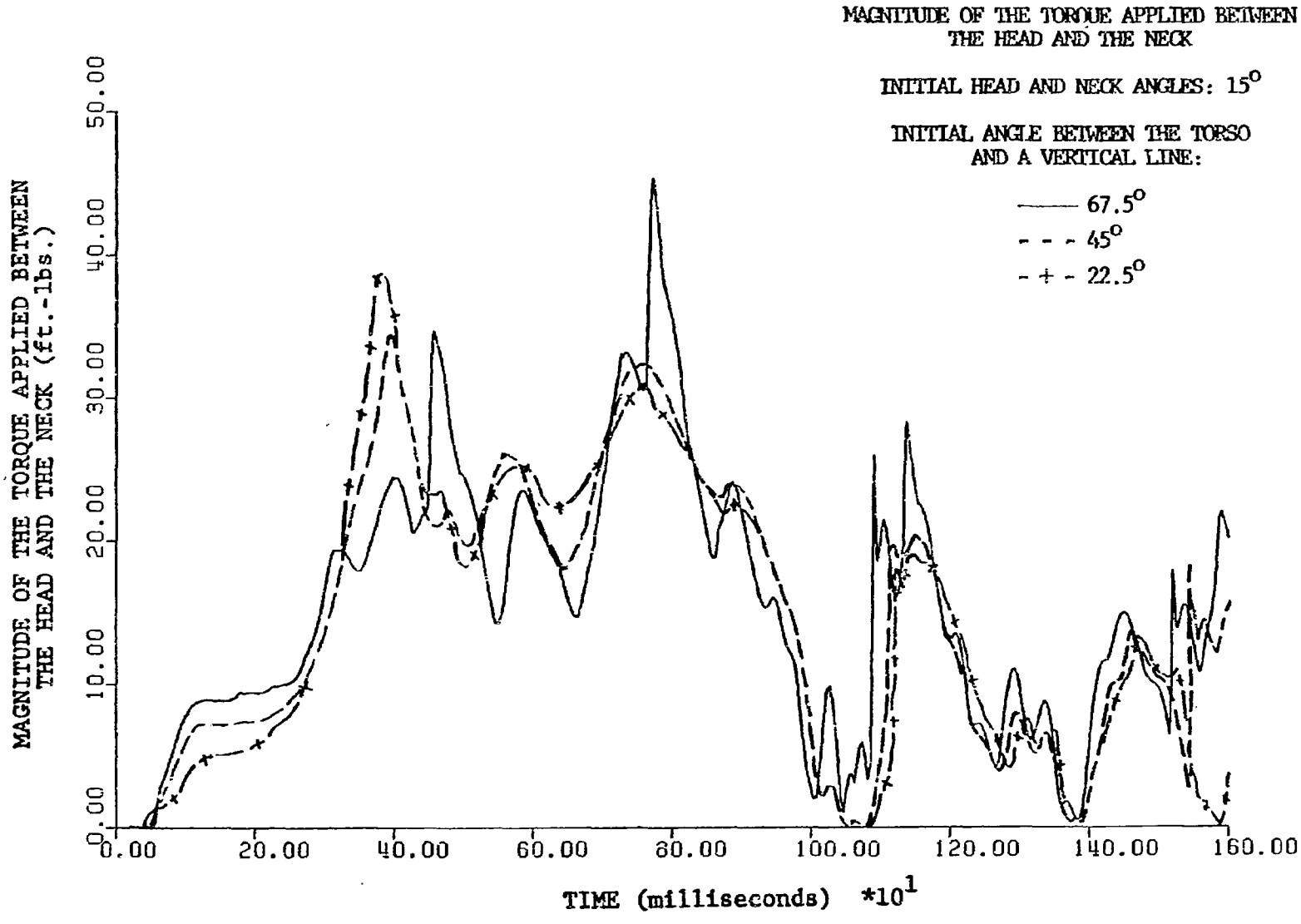

Figure 38. Magnitude of the Torque Applied Between the Head and the Neck

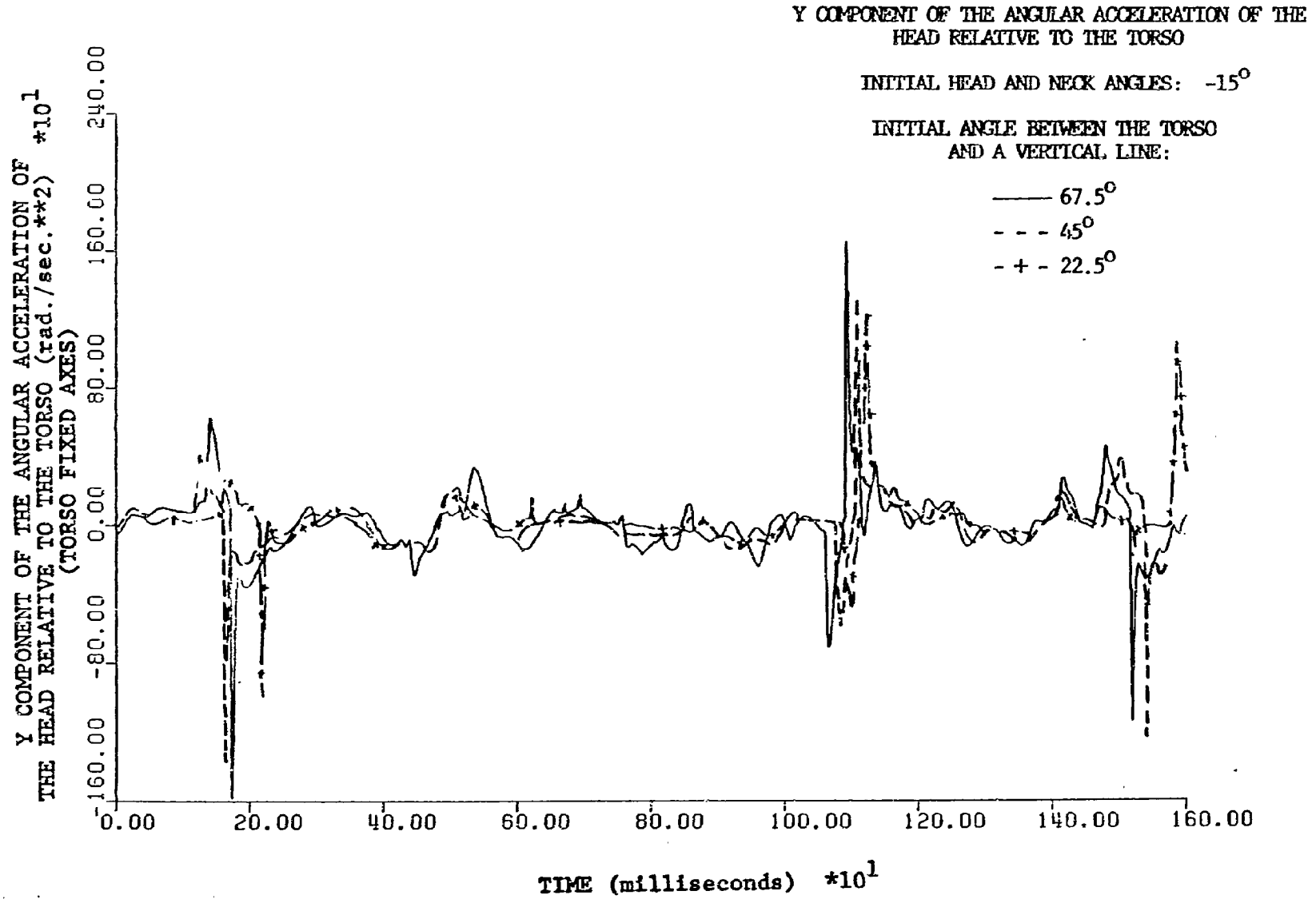

Figure 39. Y Component of the Angular Acceleration of the Head Relative to the Torso

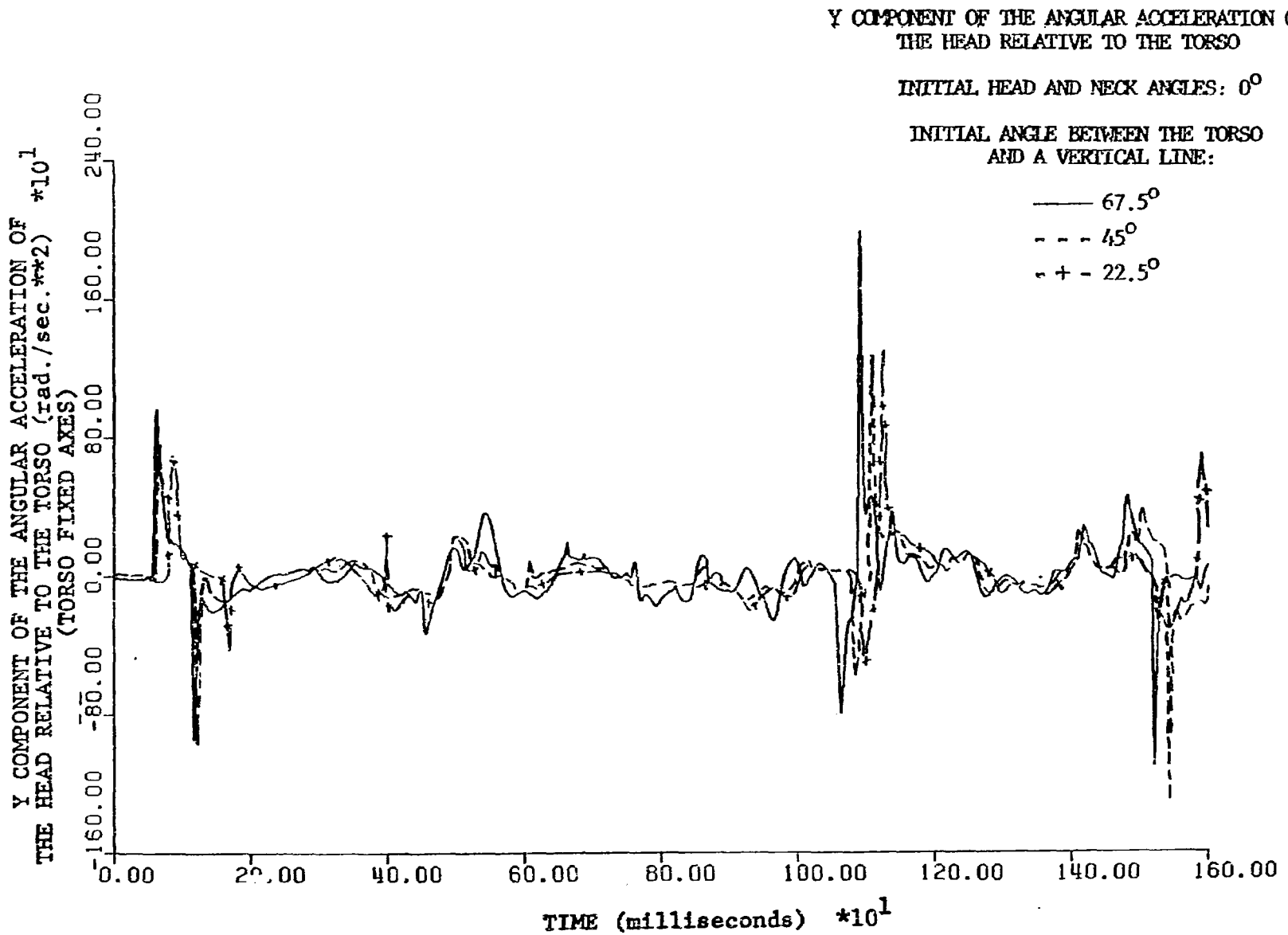

Figure 40. Y Component of the Angular Acceleration of the Head Relative to the Torso

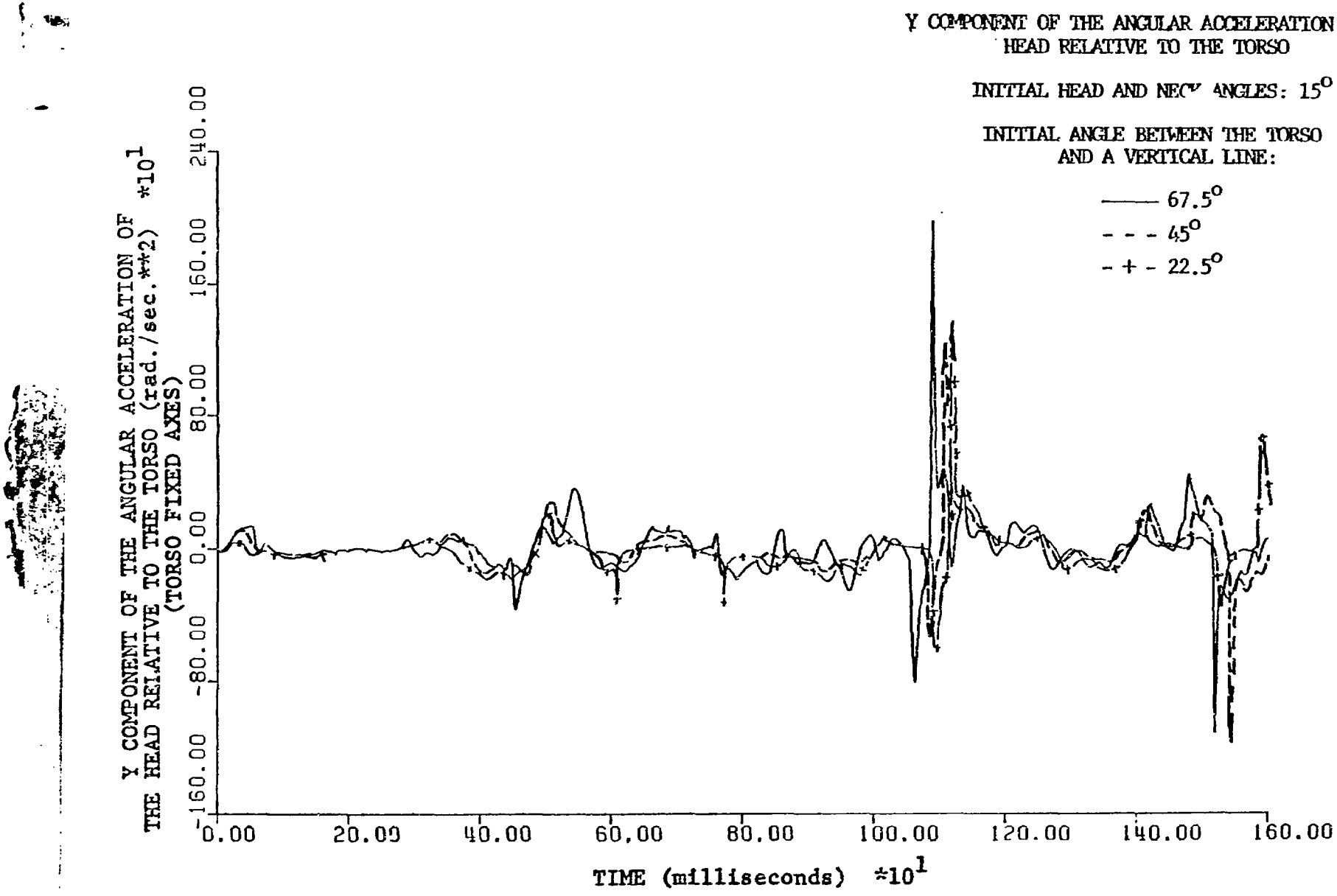

Figure 41. Y Component of the Angular Acceleration of the Head Relative to the Torso

REFERENCES

1. Palmer, J. F., and Call, D. W., "Data Reduction of Physical Forces Related to Physiological Stress of Parachutes," Research paper of work unit MF12.524 EN037 of Navy Bureau of Medicine and Surgery, 1975.

2. Call, D. W., Palmer, J. F., and Ewing, C. L., "Human Head and Neck Response to Multi-Axis Accelerations During Military Parachuting," Research paper of work unit MF51.524 005 702DA/J Navy Bureau of Medicine and Surgery, 1975.

3. Heinrich, H. G., and Saari, D. P., "Parachute Opening Shock Calculations with Experimentally Established Velocity and Area Functions," AIAA Paper No. 75-1382, AIAA 5th Aerodynamic Deceleration Systems Conference, 1975.

4. Woolman, R. D., "Performance Data for Four Free-Type Back-Style, Automatic Personnel Parachute Assemblies," Report No. AFFTC-TR-74-35, Air Force Flight Test Center, Edwards AFB, CA, 1975.

5. Huston, R. L., Winget, J. M., and Harlow, M. W., "Biodynamic Model of a Parachutist," Aviation, Space and Environmental Medicine, January, 1978, pp. 178-182.

6. Huston, R. L., "Three-Dimensional, Gross Motion, Crash-Victim Simulators," Structural Mechanics Software Series, Vol. I, University Press of Virginia, 1977, pp. 611-622.

7. Huston, R. L., Hessel, R. E., and Winget, J. M., "Dynamics of a Crash Victim - A Finite Segment Model," AIAA Journal, Vol. 14, No. 2, 1976, pp. 173-178.

8. Huston, R. L., Passerello, C. E., and Harlow, M. W., "UCIN Vehicle - Occupant/Crash Victim Simulation Model," Structural Mechanics Software Series, University Press of Virginia, Vol. 22, 1978, pp. 131-150.

9. Huston, R. L., Passerello, C. E., Hessel, R. E. and Harlow, M. W., "On Human Body Mechanics," Annals of Biomedical Engineering, Vol. 4, 1976, pp. 25-43.

10. Huston, R. L., Passerello, C. E., Harlow, M. W., and Winget J. M., "The UCIN 3-Dimensional Aircraft Occupant," Aircraft Crashworthiness, University Press of Virginia, 1975, pp. 311-324.

11. Young, R. D., "A Three Dimensional Mathematical Model of an Automobile Passenger," NTIS Report No. PB 197159, August, 1970.

12. Kane, T. R., Dynamics, Holt, Rinehart, and Winston, New York, 1968.

13. Kane, T. R., "Dynamics of Nonholonomic Systems," Journal of Applied Mechanics, Vol. 28, 1961, pp. 574-578.

14. Huston, R. L., and Passerello, C. E., "On Lagrange's Form of d'Alembert's Principle," The Matrix and Tensor Quarterly, Vol. 23, No. 3, March, 1973, pp. 109-112.

15. Huston, R. L., Passerello, C. E., Harlow, M. W., and Winget, J. M., "User's Manual for UCIN-SUPER:CHAIN SYSTEMS," NTIS Report PB247059, 1975.

16. Huston, R. L., Passerello, C. E., and Harlow, M. W., "Dynamics of Multi-Rigid-Body Systems," Journal of Applied Mechanics, Vol. 45, December, 1978, pp. 889-894.